NASA CONTRACTOR REPORT 166339

NASA-CR-166339
19820017493

The Relative Stress-Corrosion-Cracking Susceptibility of Candidate Aluminum-Lithium Alloys for Aerospace Structural Applications

Patrick P. Pizzo

Advanced Research and Applications Corporation

CONTRACT NAS2-10365
September 1980

NF02612

NASA

NASA CONTRACTOR REPORT 166339

The Relative Stress-Corrosion-Cracking Susceptibility of Candidate Aluminum-Lithium Alloys for Aerospace Structural Applications

Patrick P. Pizzo

Advanced Research and Applications Corporation
1223 E. Arques Avenue
Sunnyvale, California 94086

Prepared for
Ames Research Center
under Contract NAS2-10365

National Aeronautics and Space Administration

Ames Research Center
Moffett Field California 94035

TABLE OF CONTENTS

LIST OF ILLUSTRATIONS

LIST OF TABLES

ABSTRACT

The aging response of two powder metallurgy (P/M) processed aluminum-lithium alloys has been determined. Alloy I has the composition of Al-2.6% Li-1.4% Cu. Alloy II is the same as Alloy I but also contains 1.6% Mg. Yield and ultimate tensile strengths of 480 MPa and 550 MPa were obtained for Alloy I after a peak age of 26 hours at 443K. Higher yield and ultimate strength of 525 MPa and 580 MPa were obtained for Alloy II after a peak age of 26 hours at 463K. Strain-to-fracture was comparable for both alloys at about 3%. Some improvement in tensile ductility was achieved at the sacrifice of tensile strength by varying the solution heat treatment temperature or by under-aging or over-aging. In general, fracture characteristics were brittle, and limited reduction-in-area was observed in both alloys. The fracture mode and morphology of the two alloys differed. Alloy I fractured by transgranular separation (slip-plane decohesion) along a plane of maximum shear stress. Alloy II fractured by intergranular separation along a plane of maximum tensile stress. A fixed orientational relationship was found to exist between the shear fracture plane of Alloy I specimens and the rolling direction, thus suggesting that this P/M alloy may be strongly textured. Alloy II exhibited recrystallization and grain growth, as well as coarse precipitation along grain boundaries. The aging response of both alloys was found to be sensitive to hot working operations performed prior to solution heat treatment.

INTRODUCTION

Over the next decade, emphasis will be placed on the development of advanced aluminum alloys for aerospace structural applications.[1,2] Advanced alloys will be utilized in the design or major redesign of space, missile and aircraft systems. Alloys will be tailored in terms of: 1) density, 2) elastic modulus, and 3) strength to achieve major savings in weight and, thus, reduce operational expense. To fully assess the strength-to-weight or stiffness-to-weight advantage of the candidate alloys, durability criteria, such as fatigue endurance and/or environmental degradation, must be assessed. Stress corrosion cracking (SCC) of high-strength aluminum alloys has been a prevalent service problem in the aircraft industry. Thus, the strength-to-weight advantage for an alternative alloy needs to be normalized in terms of susceptibility to SCC. The purpose of the current research program is to: 1) identify a practical SCC screening technique, and 2) evaluate the relative SCC resistance of Al-Li candidate advanced aluminum alloys. This work is essential for successful near-term use of improved alloys for commercial systems and for the eventual development of optimum structural alloys.

The objective of this first report is to characterize the microstructure and tensile properties of the two aluminum-lithium alloys selected for study. The alloys were produced using the powder metallurgy technique. Due to the unique chemistry and fabrication history of the alloys, the decision was made to 1) investigate the aging response and 2) establish baseline tensile properties. The aging response was studied to determine the heat treatment sequence which will yield optimum mechanical properties. Particular attention was focused on achieving sufficient tensile elongation at high tensile strength so that degradation under SCC conditions could be properly assessed. The fracture morphology under ambient conditions was also characterized for later comparison to SCC features.

BACKGROUND

The two most widely used structural aluminum alloys in the aerospace industry are the Al-Cu base alloy 2024 (Aluminum Association designation) and the Al-Zn-Mg-Cu base alloy 7075. In the aged condition (-T3 and -T4 for 2024 aluminum and -T6 for 7075 aluminum), the alloys are characterized by low smooth specimen SCC threshold stress values (< 55 MN/m^2) in the short-transverse direction.[3] This low resistance to SCC has resulted in a high frequency of service problems. Through manipulation of minor element chemistry and through alternate temper treatments (overaging treatments), the SCC resistance of these alloys has been improved, but usually at the expense of reduced tensile properties. Additional progress has been made to introduce improved alloys through adjustment of alloy chemistry and through thermomechanical treatment (TMT). However, conventionally-processed (cast ingot metallurgy) alloys fall short of demonstrating sufficient improvement in properties to displace the two mainstay alloys of the aerospace industry; the 2XXX and 7XXX series alloys.

Better combinations of strength, resistance to stress corrosion cracking and resistance to exfoliation corrosion can be obtained in wrought products made from pre-alloyed atomized powder than in corresponding products made from cast ingot.[2,4,5] Improvements are attributable to the unique microstructure of the rapidly solidified powders. Microstructural advantages include 1) decreased grain size (grain sizes less than 1 μm are attainable), 2) increased solid solubility (often by orders of magnitude when compared to equilibrium conditions), and 3) elimination of segregated phases. In the United States, microstructural characterization of several base systems is proceeding. Aluminum alloys that have been investigated include: Al-Cr, Al-Cu, Al-Fe, Al-Co, Al-Ni, Al-Mn, Al-Zr, Al-Hf, Al-Fe-Mn, and Al-Mg-Mn.[2] Microstructure and mechanical properties measurements on consolidated material are also being conducted. The following alloys have been studied: Al-Cu-Mg (2024), Al-Zn-Mg (7075), Al-Fe, Al-Mn-Cu, Al-Mn, Al-Cu-Mg-Li (2024 + lithium), Al-Li, Al-Cu-Li and Al-Mg-Li.[1,2,5,6,7]

Alloy MA87, similar in composition to 7075 aluminum, is an example of the potential alloy advancement available through P/M techniques. In comparison with the ingot metallurgy (IM) 7075 aged to similar longitudinal yield strength, P/M alloy MA87 exhibits an approximate 15% improvement in tensile strength, a 20% improvement in the fatigue endurance limit, a reduced fatigue crack growth rate, and a 100% increase in the resistance to stress corrosion.[5] Powder metallurgy technology offers a broad range of compositional variation, unattainable through conventional cast ingot processing. Thus, the greatest potential for significant advancement in aluminum aerospace alloys may be provided by P/M processing technology.

Of the many candidate aluminum structural alloys being developed using P/M technology, aluminum-lithium alloys offer the best potential for successful near-term use in the aerospace industry. Al-Li alloys are prime candidates because they offer significant increases in specific modulus (i.e., elastic modulus to density ratio), while providing strength similar to the 7XXX series and 2XXX series I/M alloys.[1,7] Because difficulties have been experienced in conventional casting, alloy X-2020 (Al-4.5 Cu-1.5 Li)* was withdrawn as a commercial product in the late 1950's. Recent attention has focused on producing Al-Li alloys from rapidly solidified powders.[2,6]

Two powder metallurgy processed Al-Li alloys have been procured for the SCC study. The alloys are Al-2.6% Li-1.4% Cu and Al-2.6% Li-1.4%Cu-1.6% Mg. Both compositions are of potential commercial interest because of the high specific strength values attainable. In addition, the presence of magnesium in the latter alloy alters the precipitation kinetics and influences the size and distribution of the grain boundary precipitates. Since grain boundary precipitates and/or the accompanying precipitate free zones (PFZ's) are thought to play an important role in the stress corrosion cracking process, the influence of the Mg addition will be closely monitored.

*All compositions in weight percent

EXPERIMENTAL TECHNIQUE

Two aluminum-lithium alloys were purchased from Kawecki Berylco Industries, Inc., Reading, Pennsylvania. The alloys were processed using powder metallurgy (P/M) techniques. Powders were produced by rapid cooling an atomized molten stream of the target composition in an inert gas (Ar) atmosphere. High-purity (0.9999 weight percent) aluminum and a 20 wt. pct. lithium master alloy were combined so as to yield an approximate 2.6 wt. pct. aluminum-lithium melt. High purity element additions were made to adjust the melt to the desired alloy composition. The cooling rate of the atomization process was estimated to be approximately 10^3 ^oK/sec. The resulting powders were spherical, about 150 m in diameter (sized to 100 mesh).

Powders were packed in 6061 aluminum cans (13.7 cm O.D. with a 0.32 cm wall) and cold isostatic pressed to 415 MPa. The compacted powders were then hot upset at 755^oK against a blind die and extruded at 672^oK through a 55.9 mm by 14.7 mm (2.2 inch by 0.58 inch) die. This yields an approximate 10:1 extrusion ratio.

The chemical compositions of the resulting alloys are presented in Table I. The lithium content was determined using the wet chemical technique. The zirconium is added to refine grain size and to retard grain growth. The Al- Li- Cu alloy is hereafter designated Alloy I. The Al- Li- Cu- Mg alloy is hereafter designated Alloy II.

Microstructures representative of the as-received alloys are presented in Figure 1. Coarse precipitation is observed in both alloy systems and this results from the somewhat high processing temperatures used in the consolidation of the powders. The precipitation in Alloy II is particularly coarse. Precipitation is found to be preferentially in lines parallel to the extrusion direction (ED) in both alloys, although the effect is most notable in Alloy I.

To scope the aging response of the alloys, hardness testing was conducted on coupon specimens 12 mm by 8 mm by 1.5 mm, cut from hot rolled strip. The strip was hot rolled at about 700°K with rolls maintained at 450°K. The section thickness was reduced about 5% per pass, and the material was reheated to 700°K after every four passes. In this manner, a 1.5-mm-thick strip was prepared from the 14.7 mm thick original extrusion and was also used to make tensile specimens for characterization of the mechanical properties. The Rockwell 15-T superficial hardness scale was used to measure hardness.

Tensile tests were performed using the three specimen types depicted in Figure 2. The tensile coupons, Figure 2a, were also fabricated from the hot rolled strip. The straining electrode specimens (for the subsequent stress corrosion study), Figure 2b, and the tensile rounds, Figure 2c, were fabricated from the extruded plate. All heat treating was performed in air after specimen fabrication. Specimens were rough-polished to 600 grit abrasive paper prior to testing. Tensile tests were performed using a closed loop electrohydraulic test system under stroke control. Tensile tests were conducted under ambient conditions at a measured plastic strain rate of $1.4 \times 10^{-4} S^{-1}$. Modulus determinations were made from the output of two strain gauges attached to opposite sides of tensile coupons, Figure 2a. An extensometer was used to determine engineering strain, e, to final fracture. The strain-to-fracture, ^{e}f, data reported herein are the values of the plastic engineering strain-to-fracture determined from the displacement versus load record.

RESULTS AND DISCUSSION

In this section, the microstructure, aging response, and tensile properties of the two aluminum-lithium alloys are characterized. First, attention is focused on microstructural changes occurring as a result of heat treatment and hot rolling. Solution heat treatment was necessary to dissolve the coarse $\delta(Al_3Li)$ precipitates found in the as-received material and condition the alloy for peak age-hardening. Second, the aging data are presented. Time and temperature conditions for peak strengthening are defined for each alloy. Next, the tensile properties of Alloys I and II are presented as a function of heat treatment. The purpose of these data is to establish strength/ductility combinations which are most pertinent for the subsequent investigation of stress corrosion cracking. Finally, the morphology of room temperature fracture is also characterized to assist interpretation of the tensile results and for later comparison to fractures induced by stress corrosion cracking.

Microstructure

Solution heat treatment was performed to dissolve the coarse precipitates found in the P/M processed alloys. Preliminary scoping tests indicated that the precipitates begin to go into solution at temperatures somewhat greater than 670°K. This is consistent with the solubility data for the binary Al-Li alloy system reported by Costas and Marshall.[8] Thorough dissolution of precipitates within 0.5 hours occurred for temperatures greater than 780°K. Solution heat treat conditions ranging from 768° to 828°K are investigated in this study.

Aging Response

Many aluminum alloys exhibit age hardening due to the growth of metastable phases that result from decomposition of the supersaturated solid solution. The metastable phase responsible for strengthening in Al-Li binary alloys is an ordered Al_3Li precipitate, termed δ'. [9,10] Under certain conditions of time and temperature, the precipitation of δ' is homogeneous, producing a high density of very small ($\sim$.010μm diameter) spherical precipitates. In Al-Li-Cu ternary alloys, the lithium precipitates independently of copper which follows the sequence that occurs in the Al-Cu binary system:

$$GPI \longrightarrow GPII \longrightarrow \theta'' \longrightarrow \theta' \ (Al_2Cu)$$

Both the δ' and the θ'' precipitates effectively impede dislocation motion, causing an increase in flow strength. However, continued aging results in progressive loss in coherency between the matrix and the precipitate as the metastable δ' transitions to δ phase and as the θ'' proceeds toward the equilibrium θ'. As a consequence, there is a reduction in yield and tensile strength, as predicted by mechanisms such as the one proposed by Orowan. [11] Maximum strengthening thus occurs at some intermediate aging time that is dependent, in part, on alloy chemistry. In this section, data which characterize the aging response of the two alloys are presented.

The microstructures of Alloy I and II, after solution heat treatment at 828°K for 0.5 hours, are presented in Figures 3 and 4. Linear indications present in the original extrusion remain decorated with precipitates. Recrystallization is observed in both alloys. The larger recrystallized grains are about 30μm long in the extrusion direction, while growth in the short transverse direction appears constrained by the linear array of precipitates. The array of precipitates is linear rather than planar. This is also evident in the transverse section micrographs of Figure 4. A relatively uniform array of precipitates is observed in the transverse field. The recrystallized grains are rather equiaxed and of the approximate dimension of the spacing of the linear indications in the longitudinal section. The linearly-aligned precipitates of Figure 3 are thought to be zirconium. This will be investigated in later work.

The microstructure of the hot rolled strip after 828°K/0.5-hour solution heat treatment and subsequent aging is presented in Figure 5 for Alloy I and in Figure 6 for Alloy II. Both longitudinal and transverse sections are presented. Alloy I is found to retain microstructural features refined by the hot rolling process. Grains and/or sub-grains approximately 5μm in size are observed in Figure 5b. On the other hand, extensive recrystallization and grain growth is observed in the magnesium-containing alloy, Alloy II. The structure of Alloy II consists of large grains (> 100μm diameter) amongst local clustering of smaller, equiaxed grains. Coarse precipitates are observed along grain boundaries. The possibility of heterogeneous precipitation of a grain boundary phase will be investigated in a subsequent transmission electron microscopy study. Large (60μm long) particles, such as that in Figure 5a, are present in both aluminum-lithium alloys. Energy dispersive analysis (KEVEX) indicates the particles contain Al and/or Li. The particles may relate to the master alloy addition and are probably

carryovers from the melt during the atomization process. The point of fracture initiation in approximately 10% of the tensile tests was associated with such particles.

The aging response of Alloys I and II is presented in Figures 7 through 9. Figure 7 is a plot of hardness as a function of aging temperature for a constant aging time of 16 hours. These data define the temperature regime where the δ'/θ'' precipitation is rapid; they also provide a measure of the relative strength difference between Alloys I and II. Figures 8 and 9 show the variation in hardness with time for two aging temperatures; 443°K and 463°K respectively. Since hardness is a measure of the yield and flow strength of an alloy, the data indicate time/temperature conditions for maximum strengthening. The data of Figure 7 indicates that accelerated strengthening occurs at a higher temperature for the magnesium bearing alloy, Alloy II. For a fixed aging time, maximum hardening occurs at 450°K for Alloy I and at 470°K for Alloy II. The magnesium addition appears to alter the precipitation process and increase the strength of the base alloy. On the basis of the data of Figure 7, aging temperatures of 443°K and 463°K were selected for the time-at-temperature aging study. The time dependence of hardness for aging Alloys I and II at 443°K and 463°K are reported in Figures 8 and 9, respectively. Peak hardness for Alloy I occurs in about 30 hours at 443°K. Alloy II reaches full hardness in about 200 hours at this temperature. At 463°K, Alloy I is peak aged in about 5 hours while Alloy II requires 40 hours to attain maximum hardness. The addition of magnesium is again demonstrated to increase alloy strength and to alter precipitation kinetics.

Tensile Properties and Fracture Morphology

The goal of this study was to develop a heat treatment which will render the reference alloys high strength and yet maintain sufficient and reproducible ductility, about 6%, to perform the SCC investigation. In this section, the baseline tensile properties of Alloys I and II are presented as a function of aging condition. The tensile properties are characterized in Figures 10 thru 14 and in Table 2.

In Figures 10 and 11, the yield strength (0.2% offset), ultimate tensile strength and plastic strain-to-fracture versus aging time curves for Alloys I and II, respectively, are presented. Tensile coupons, Figure 2a, were used. Curves for $443^{o}K$ and $463^{o}K$ aging are presented in each figure. The following trends are observed:

1) The largest value of strain-to-fracture at relatively high strength is 5% for Alloy I and 6% for Alloy II.
2) While the strain-to-fracture, e_f versus $443^{o}K$ aging curve for Alloy I (Figure 10) goes through a minimum as peak aging is approached, the $463^{o}K$ aging curve for e_f exhibits an unexpected maxima.
3) The e_f versus $463^{o}K$ aging curve for Alloy II exhibits a local maxima at about 14 hours. As the peak strength is more closely approached, the strain-to-fracture rapidly decreases.
4) The yield strength and ultimate tensile strength versus aging time curves of Figures 10 and 11 correlate well with the hardness versus aging curves of Figures 8 and 9. Aging peaks occur at similar aging times.

The data of Figures 10 and 11 point out the necessity for close control of aging conditions because of the anamolous behavior of the ductility parameter, e_f. The optimum e_f value of 5% for Alloy I can be attained either by peak aging at $463^{o}K$ or by overaging at $443^{o}K$. A strain-to-fracture value of 6% results when Alloy II is underaged, but if aging proceeds too far, the strain-to-fracture rapidly declines to about 3%. Aging temperatures somewhat greater than $463^{o}K$ are expected to shift the aging response curve to the left such that the decline in e_f with time may occur for significantly shorter times. The reproducibility of ductility parameters is a major concern in the SCC study. Therefore, the e_f for selected heat treatments will require a statistical base to define reproducible control conditions.

To determine Young's modulus, E, strain gauges were mounted on two sides of the flat tensile coupons. Moduli are reported in Table 2. A value of 80 GPa is consistent with the data of Webster on alloys of similar composition. [12] The modulus for 7075-T6 aluminum is included for comparison. The reference aluminum-lithium alloys are 12% stiffer than 7075-T6 aluminum.

The morphology of the fractured tensile test specimens was studied for later comparison to stress corrosion fracture surfaces. Photographs of the tensile coupon fractures are presented in Figures 12 thru 16.

Alloys I and II were observed to fail in distinctly different manners as illustrated in Figure 12 where typical fracture surfaces are shown. Figure 12a is a comparison of the fracture profile of Alloy I (top) and Alloy II fractures. Alloy I fails by shear (47.5^{o} measured with respect to the load axis) while Alloy II fractures on a plane perpendicular to direction of maximum load. Shear fractures for Alloy I and tensile fractures for Alloy II were observed for the specimens used to generate the data of Figures 10 and 11. Comparison of the fracture surfaces of Alloys I and II is presented in Figure 12b. The variation in fracture topography is clearly observable.

In Figures 13 and 14, scanning electron micrographs (SEM) showing the fracture topography of Alloy I specimens are presented. A stepped, brittle fracture appearance is observed. Elongated dimples, characteristic of ductile metals failed by shearing, are not observed.

SEM micrographs of the fracture surface of Alloy II specimens are presented in Figures 15 and 16. The fracture of the magnesium-bearing alloy contains laminar tears oriented parallel to the rolling plane. The tears are thought to occur along interfaces weakened during processing of the hot rolled strip. In substantiation, fracture surfaces of Alloy II specimens fabricated from the as-received extrusion do not exhibit laminar tears. Intergranular facets approximately 5μm in size are the predominant fractographic feature.

Both Alloy I and Alloy II fractures exhibit less than 3% reduction in area . In addition, final fracture of the tensile specimens occurs at the point of plastic instability (maximum load). These data combined with the SEM fractographic results demonstrate the brittle nature of fracture in both alloys.

The tensile data of Figures 10 and 11 represent Al-Li alloy solution heat treated at 828°K. In Figures 17 and 18, tensile properties are presented as a function of solution heat treatment temperature for a constant aging condition. These data were obtained using tensile round specimens, Fig. 2(c), which were fabricated directly from the extruded plate. The objective of these tests was to determine the solution heat treatment (SHT) which provides optimum ductility for each of the alloys. The following results are found:

(1) The ductility of Alloy I is somewhat greater than 3% and unaffected by SHT temperature. However, the yield strength (YS) and ultimate tensile strength (UTS) are maximum at 788°K. These data suggest that the aging response of Alloy I solution heat treated at 788°K be investigated for optimum properties.

(2) The ductility of Alloy II decreases and the strength values, YS and UTS, increase as the SHT temperature is increased. Thus, the optimum SHT is a compromise between strength and ductility requirements. SHT at 788°K produces material with 469 MPa yield strength, 550 MPa ultimate tensile strength, and an elongation-to-fracture value of 5%; excellent tensile properties.

(3) Values of strength for the 828°K SHT condition for both alloys are higher than corresponding data reported for the tensile coupons. The yield strength and UTS values of Alloy I are 9% greater. For Alloy II, there is a more pronounced affect; tensile round YS and UTS data are greater by 42% and 30%, respectively. This anomaly will be discussed later in this report.

Fracture characteristics for the tensile rounds are analogous to those of the flat tensile coupons, and this is illustrated in Figure 19. Alloy I fracture occurs along the plane of maximum shear stress and Alloy II fracture occurs along the plane of maximum tensile stress. For Alloy II tensile rounds, there were two exceptions; both the specimen solution heat treated at 768°K and a specimen in the as-extruded condition fractured along the plane of maximum shear stress. This translation in fracture behavior in Alloy II is attributed to two reasons:

(1) For SHT temperatures less than 783°K, dissolution of coarse preciptates is incomplete, and recrystallization and grain growth do not occur. Thus, the as-extruded and 768°K SHT specimens

differ from the remaining Alloy II specimens in that relatively large, equiaxed grains are not present (compare Figure 1 to Figure 3).

(2) For SHT temperatures in excess of 783^{o}K, coarse grain boundary precipitation accompanies recrystallization and grain growth in the magnesium-bearing alloy. The grain boundary precipitation significantly reduces the cohesive strength of the grain boundary regions.

To demonstrate that precipitation events are preponderantly responsible for the fracture transition observed for Alloy II, and for the more basic difference in fracture behavior between Alloys I and II, consider the SEM fractographs of Figures 20 and 21. The fracture topography of Alloys I and II are compared in Figure 20. Alloy I exhibits a relatively flat, featureless topography while Alloy II fractures intergranularly. The flat featureless regions, Figure 20(a), are thought to correspond to crystallographic slip planes along which deformation is localized in the Al-Li-Cu and Al-L-Cu-Mg alloy systems. Slip is constrained to slip bands due to the ordered nature of the δ' precipitates. Slip continues until pile-up stresses are sufficient to cause slip-plane decohesion. Both alloys are thought to have a strong preferred orientation and, thus, a relatively flat fracture topography is expected.

Alloy II also deforms by localized slip. However, large, closely-spaced grain boundary precipitates are present in the microstructure due to the magnesium addition (reference the optical micrographs of Figures 4 and 6). The coarse grain boundary precipitates reduce the cohesive strength of grain boundaries. A condition is reached where stresses generated at the tip of the slip bands during deformation are sufficient

to cause grain boundary decohesion in preference to slip plane decohesion and intergranular fracture results. The coarse nature of the grain boundary precipitates and their influence on final fracture are evident in the fractographs of Figure 21.

It has been shown that the tensile properties for round specimens, Figures 17 and 18, are considerably greater than corresponding properties for the flat tensile coupons, Figures 10 and 11, for an equivalent heat treatment. Indeed, the YS and UTS values for Alloy II are respectively 42% and 30% greater in comparing tensile round and coupon data. Since there is a processing difference as well as specimen size difference, further testing was performed to investigate this anomaly.

Tensile tests were performed on straining electrode specimens, Figure 2(b), which were fabricated directly from the as-extruded alloy, providing isolation of the processing variable. The resulting data are plotted in Figures 22 and 23. Interpretation of the data for Alloy II is complicated because the specimens were inadvertently duplex aged. The specimens were aged at 443°K for the respective times indicated in Figure 23, prior to 463°K aging. The data are nonetheless presented, for some useful information is obtainable. The data of Figures 21 and 23 indicate the following:

1. With the exception of the high-yield strength of the specimen aged for 3 hours at 463°K, the tensile strength for the Alloy I straining electrode and coupon-type specimens is comparable. However, the strain-to-fracture data are not consistent with the trend curve representing coupon type specimens. A trend of increasing ductility with decreasing tensile strength is indicated.

2. The strength parameters for the Alloy II straining electrode specimens, Figure 23, are directly comparable to values determined for tensile rounds, Figure 18; that is, YS and UTS values are substantially greater than values obtained from the hot rolled tensile coupons. Processing strongly influences Alloy II properties.

3. The duplex aging greatly accelerates δ' precipitation in Alloy II. This is evident in that initial aging for short times at $445^{o}K$ (3 and 26 hours respectively), shifts the subsequent $463^{o}K$ aging response curve to shorter times. The aging peak is shifted from about 50 hours to less than three hours by duplex aging. The straining electrode specimen data in Figure 23 are consistent with an overaged condition for Alloy II.

The data of Figures 22 and 23 demonstrate the importance of processing as a control variable for the reference aluminium-lithium alloys. Variations in grain shape and size and the size and distribution of grain boundary precipitates strongly effect the mechanical behavior. Alloy II is more strongly affected because recrystallization and grain growth occur readily in this alloy, and grain boundary precipitation is apparently more extensive. Even in the case of Alloy I, where shear fracture mechanisms dominate, the data indicate the importance of the control of process history to yield reproductible ductility.

The fracture morphology of the straining electrode specimens was consistent with results obtained for coupon and tensile round specimens. Alloy I fractures were shear dominated, while Alloy II fractures occurred on a plane of maximum tensile stress. The fracture profile of an Alloy I straining electrode specimen is compared to tensile coupon fracture profile in Figure 24.

SEM fractographs representative of Alloy I and II are presented in Figure 25. The brittle shear characteristics previously reported for Alloy I were again observed. Alloy II fractures intergranularly, and again grain facets are typically 5μm in size. Secondary intergranular cracking is also observed.

Examination of the various shear fractures of the tensile characterization program suggests that there is a strong preferred orientation in the reference Al-Li alloys. This is demonstrated in the facture comparison of Figure 24 and the schematic of Figure 26. When orientations of the various tensile specimens are compared, final fracture occurs on planes preferentially oriented with respect to the rolling direction. X-ray diffraction will be used to determine the degree of texture and the preferred orientation.

SUMMARY

The reference aluminum-lithium P/M alloys do offer the potential of high strength, high modulus and low density. Strength properties of 480 MPa yield and 550 MPa ultimate tensile strength with strain-to-fracture approaching 5% can be achieved through proper thermo-mechanical treatment. However, the P/M alloys investigated are characterized by limited deformation beyond plastic instability. Very little reduction in area is observed and fracture chacteristics are brittle.

Because intergranular fracture occurs in Alloy II during tensile testing under ambient conditions, it is possible that the tensile properties of this alloy are environmentally sensitive. Thus, as a result of the tensile characterization-program, the scope of the stress corrosion study has been expanded to include slow-strain rate tests of Alloy II after pre-exposure to a high humidity environment. Also, because of the extent to which grain boundary precipitation occurs, Alloy II is anticipated to be the more stress corrosion susceptible of the two alloys.

Sufficient mechanical properties data have been generated to characterize the tensile properties of the two reference alloys. However, further tests are required to demonstrate satisfactory reproducibility of properties for specimens to be used in the stress corrosion program. The alloy processing steps and heat treatment must be somewhat refined to assure reproducible properties; in particular, strain-to-fracture characterization tests are in progress.

CONCLUSIONS

1) Strength properties of 480 MPa yield and 550 MPa ultimate tensile strength with strain-to-fracture approaching 5% can be achieved in both reference aluminum-lithium alloys selected for the stress corrosion study. These properties, combined with the high elastic modulus (80 GPa), make both compositions viable commercial candidates.

2) Reproducibility of properties requires close control of both alloy processing and heat treatment parameters. Further tests are required to demonstrate satisfactory reproducibility of properties for specimens to be used in the stress corrosion program.

3) Precipitation is more sluggish in Alloy II (Al-Li-Cu-Mg) than in the Al-Li-Cu ternary alloy, Alloy I. However, greater peak strength occurs in the magnesium-bearing alloy. A yield strength of 525 MPa and ultimate tensile strength of 590 MPa with a 3% strain-to-fracture value was attained for Alloy II. The maximum yield and ultimate tensile strength attained in Alloy I are 480 MPa and 550 MPa respectively.

4) Alloy I fractures along a plane of maximum shear stress, while Alloy II, in general, fractures on a plane of maximum tensile stress. Alloy II fractures intergranularly, while Alloy I fractures via slip-plane decohesion.

5) For equivalent thermomechanical processing, recrystallization and grain growth is more extensive in the magnesium-bearing alloy, Alloy II.

6) It appears that .09 wt. pct. Zr is insufficient to retard grain growth, particularly in the magnesium-bearing alloy.

7) The P/M aluminum-lithium alloys are characterized by limited deformation beyond plastic instability. Very little reduction in area is observed and fracture characteristics are brittle.

8) A fixed orientational relationship between tensile fracture surfaces and the rolling direction suggest that the P/M processed alloys are stongly textured. This is being investigated in ongoing study.

9) Because of the intergranular nature of fracture in tensile tests in Alloy I under ambient conditions, tensile properties may be environmentally sensitive. Slow strain rate tests will thus be performed for Alloy I specimens prexposed to a high humidity environment.

REFERENCES

1) Sanders, T. H. and Balmuth, E. S., "Aluminum-Lithium Alloys: Low Density and High Stiffness," Metal Progress, 113, Nr. 3 (1978).

2) Lewis, R. E., et. al., "A Feasibility Study for Development of Structural Aluminum Alloys from Rapidly Solidified Powders for Aerospace Structural Applications," Final Report AFML-TR-78-102, Lockheed Research Laboratory, Palo Alto, California, Contract F33615-77-C-5186 (May 1978).

3) Speidel, Markus O., "Stress Corrosion Cracking of Aluminum Alloys," Met. Trans., 6A (April 1975) p. 631.

4) Lyle, J. P., Cebulak, W. S. and Buchovecky, K. E., "Progress in Powder Metallurgy," 28, Metal Powder Industries Federation, N.Y., 1972, p. 93

5) Lyle, J. P. and Cebulak, W. S., "Program Metallurgy Approach for Control of Microstructure and Properties in High Strength Aluminum Alloys," Met. Trans., 6A (April 1975), p. 685.

6) Sankaran, K. K., "Structure and Properties of Splat-Quenched 2024-Type Al Alloys Containing Li," Ph.D. Thesis, MIT, Cambridge, Mass., 1978.

7) Proceedings of The First International Conference on Aluminum-Lithium Alloys, Stone Mountain, Georgia, May 19-21, 1980, to be published.

8) Costas, L. P. and Marshall, R. P., Trans. AIME, 224 (1962), p. 970-974.

9) Noble, B. and Thompson, G. E., Metal Science Journal, 4, No. 12, (Dec. 1968), P. 35-43.

10) Tamura, M., Mori, T. and Nakamura, T., J. of Jap. Inst. of Met., 31 (1970), p. 919.

11) Orowan, E., Nye, J. F. and Cairns, W. J., M.O.S. Armament Research Dept. Rep. (16/45), (1945), p. 35.

12) Webster, D., Met. Trans., 10A (Dec. 1979), p. 1913.

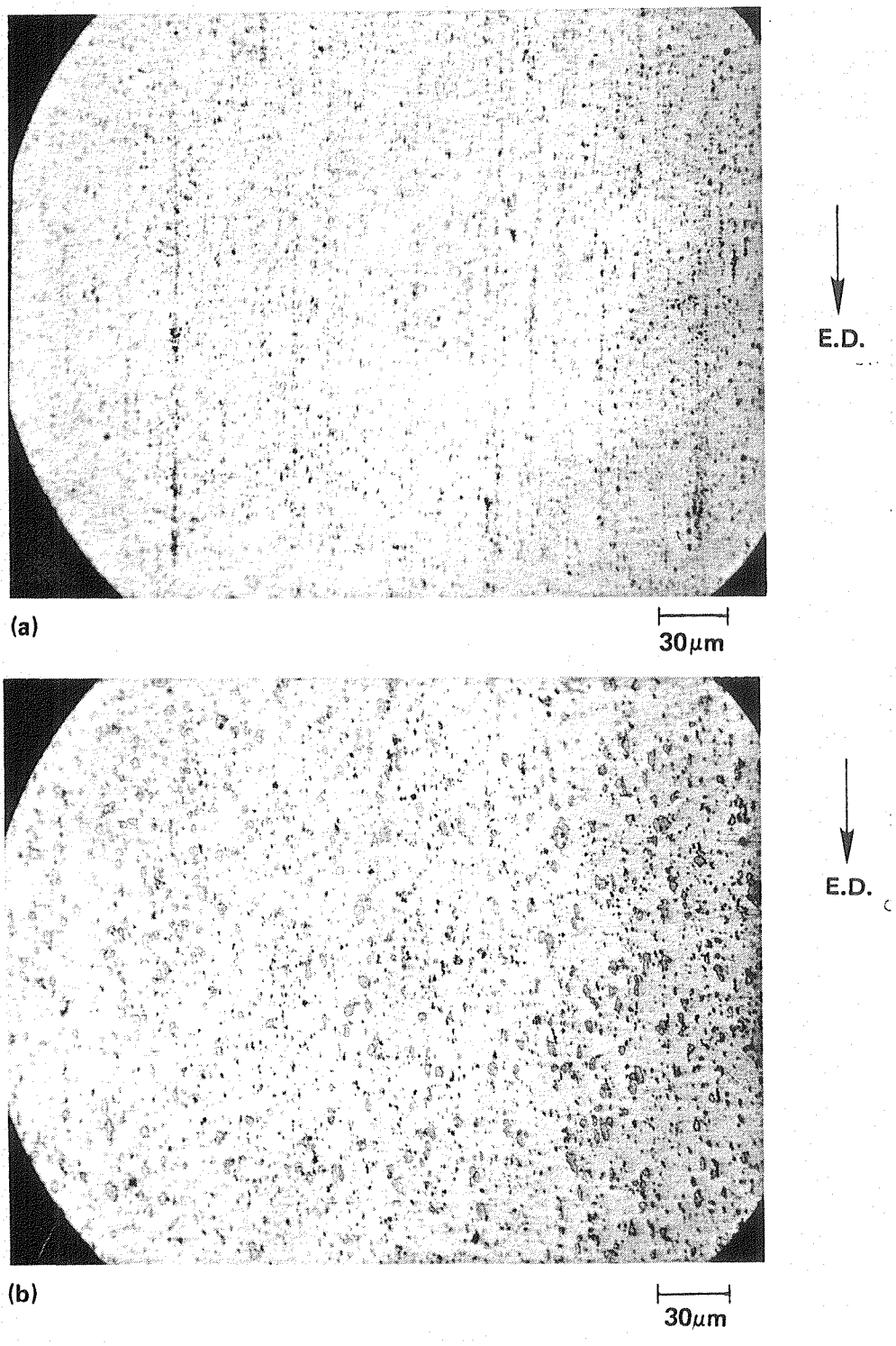

Fig. 1: Representative microstructure of the extruded plate (extrusion direction, E.D., indicated) (a) Alloy I (Al-2.6 Li-1.4 Cu) (b) Alloy II (Al-2.6 Li-1.4 Cu-1.6 Mg).

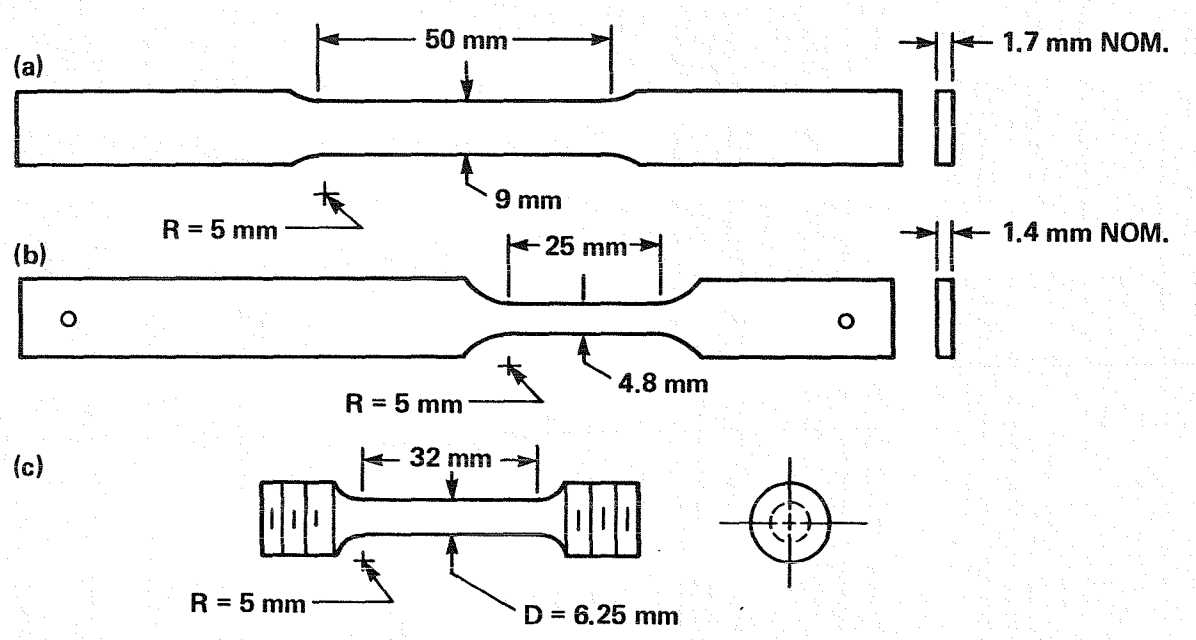

Fig. 2: Specimen types used to characterize the tensile properties of the Al-Li alloys (a) tensile coupon (b) straining electrode specimen (c) tensile round.

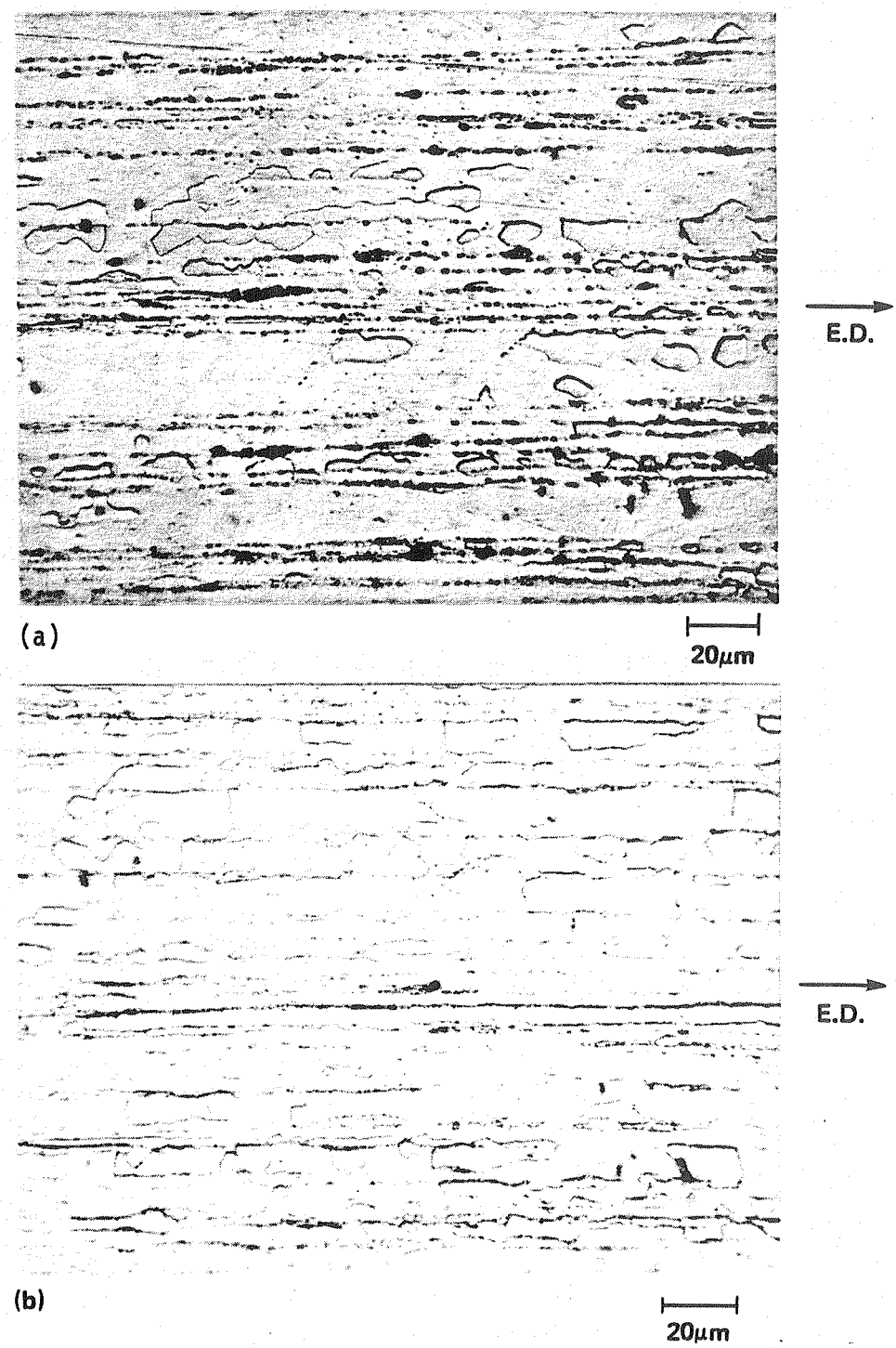

Fig. 3: Representative microstructure of the extruded Al-Li alloy plate after solution heat treatment (828K for 0.5 hours) - longitudinal sections (a) Alloy I (b) Alloy II.

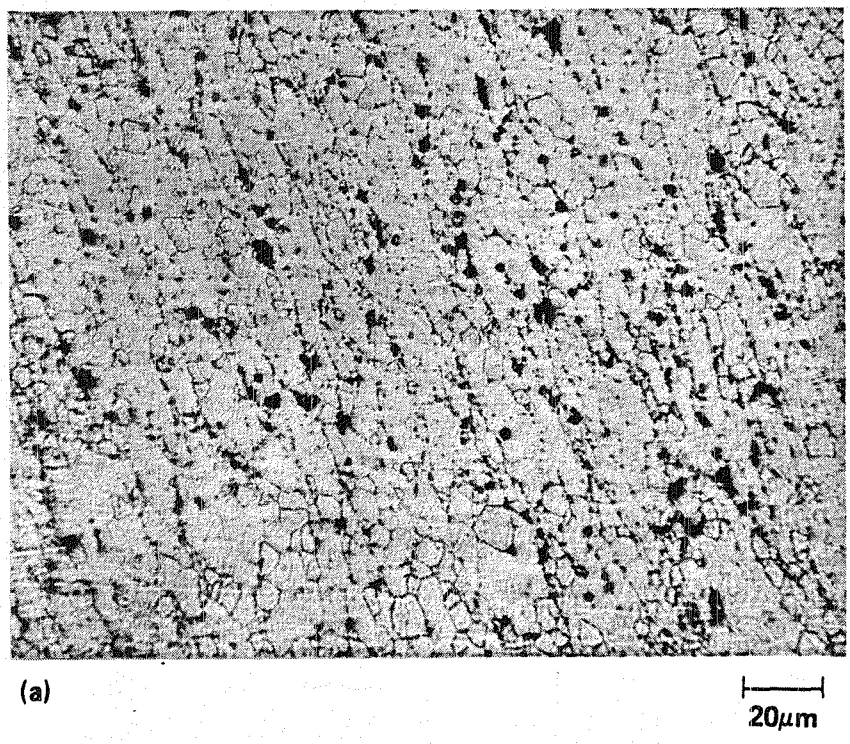

Fig. 4: Representative microstructure of the extruded Al-Li alloy plate after solution heat treatment (828K for 0.5 hours) - transverse sections (a) Alloy I (b) Alloy II.

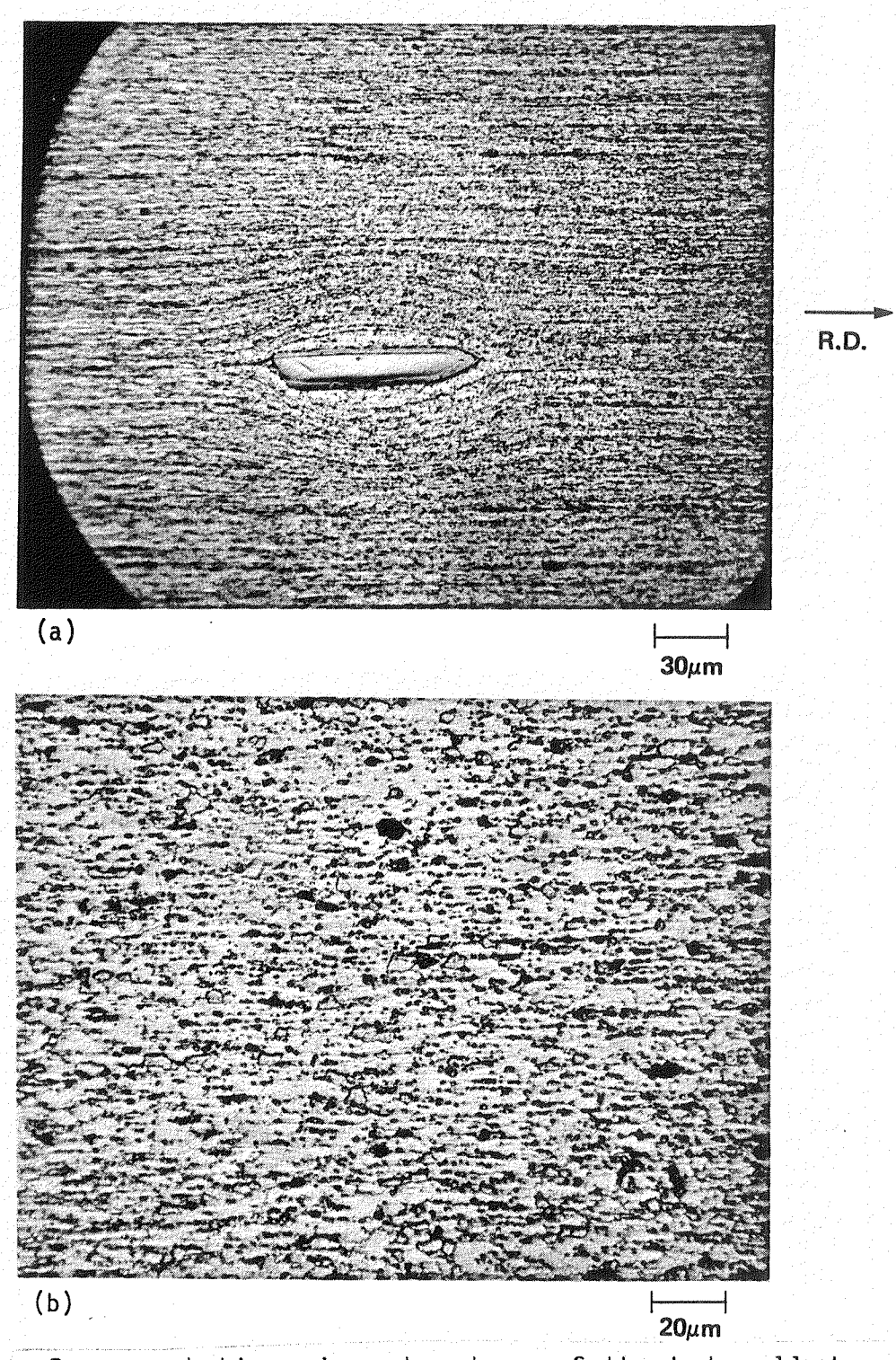

Fig. 5: Representative microstructure of the hot-rolled Alloy I sheet, solution heat treated at 828K for 0.5 hours and aged 5 hours at 463K (rolling direction, R.D., indicated) (a) longitudinal section and (b) short-transverse section.

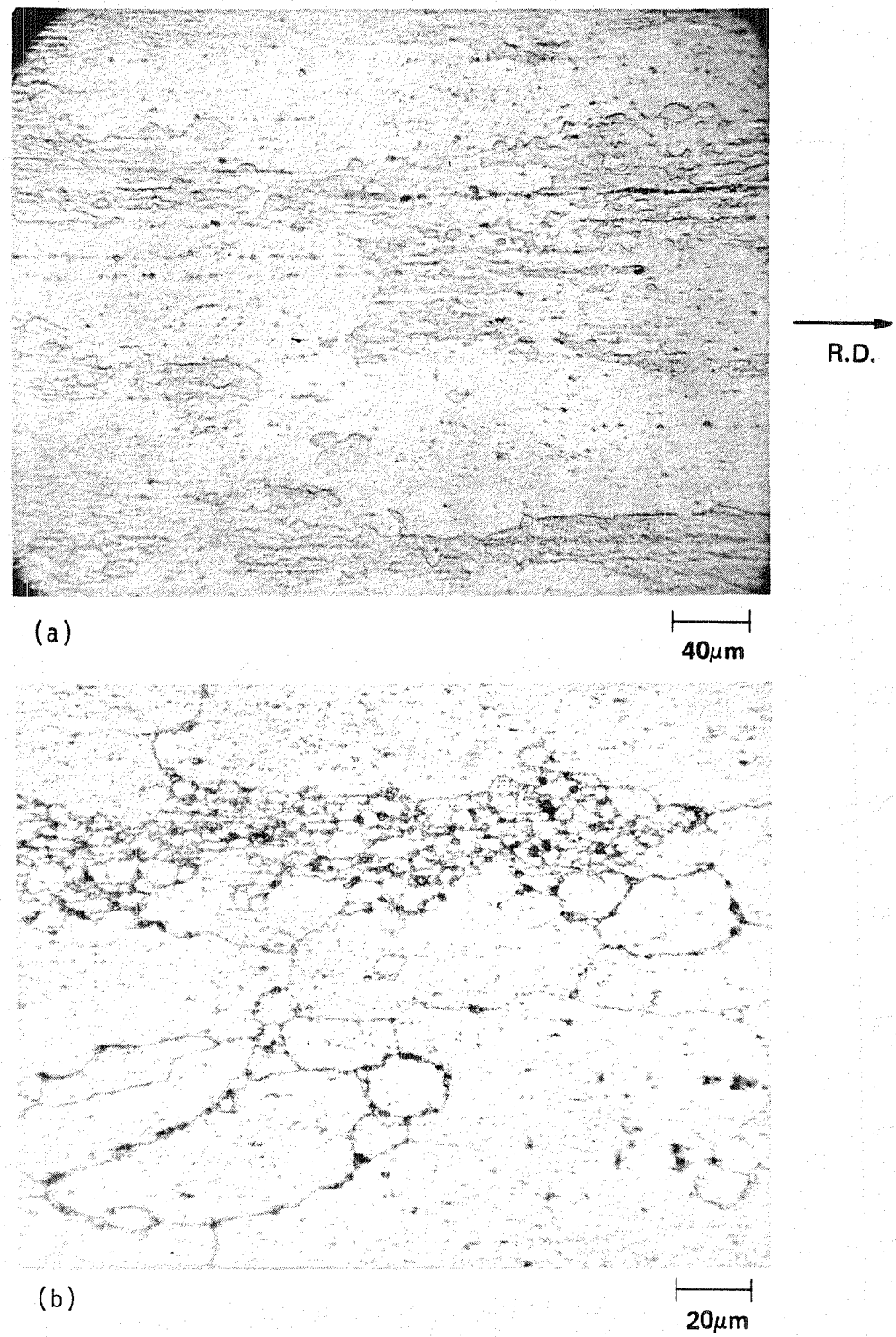

Fig. 6: Representative microstructure of the hot-rolled Alloy II (magnesium bearing alloy) sheet; solution heat treated at 828K for 0.5 hours and aged 20 hours at 463K (a) longitudinal section and (b) short-transverse section.

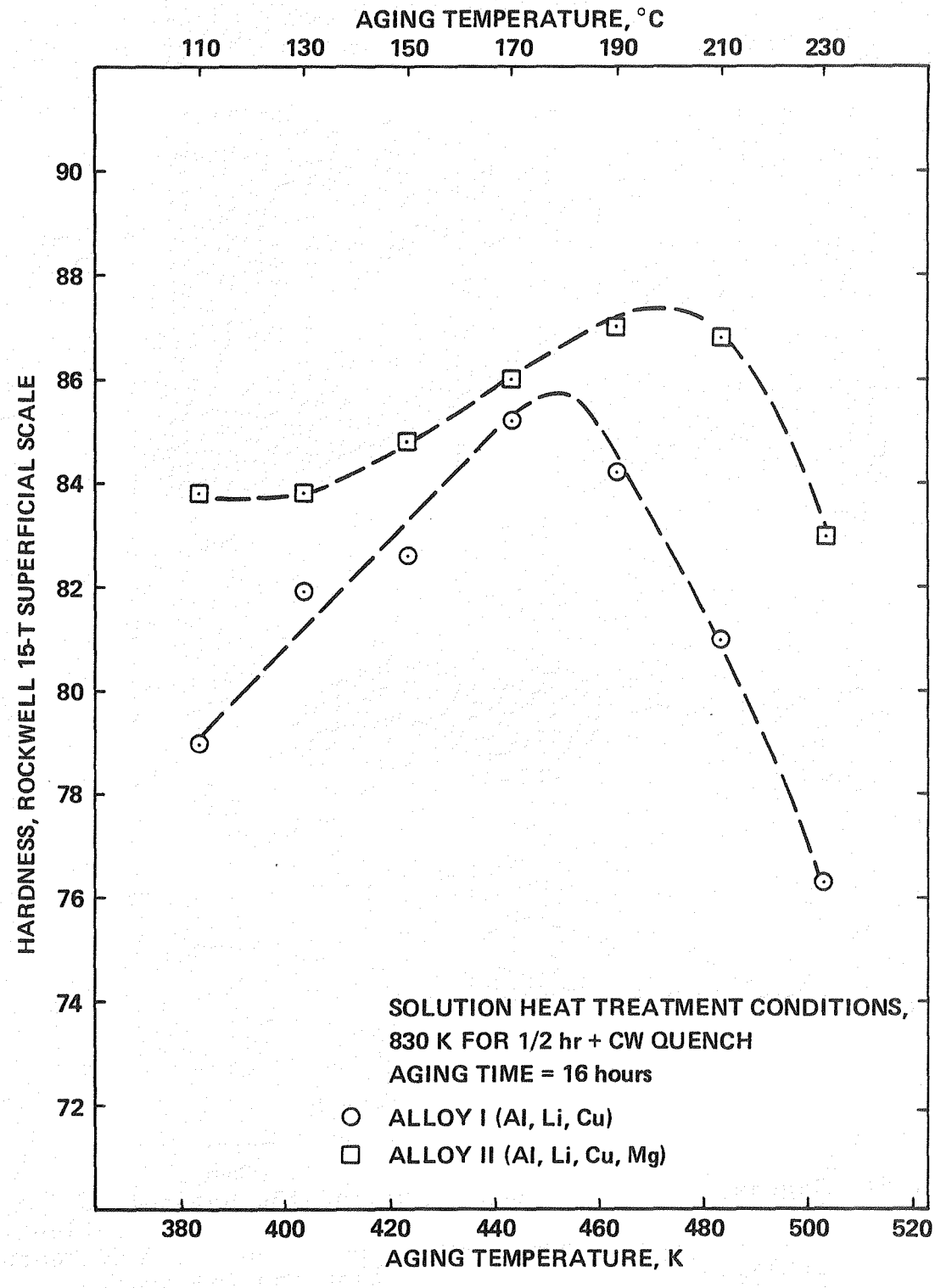

Fig. 7: Hardness as a function of aging temperature for a constant aging time of 16 hours.

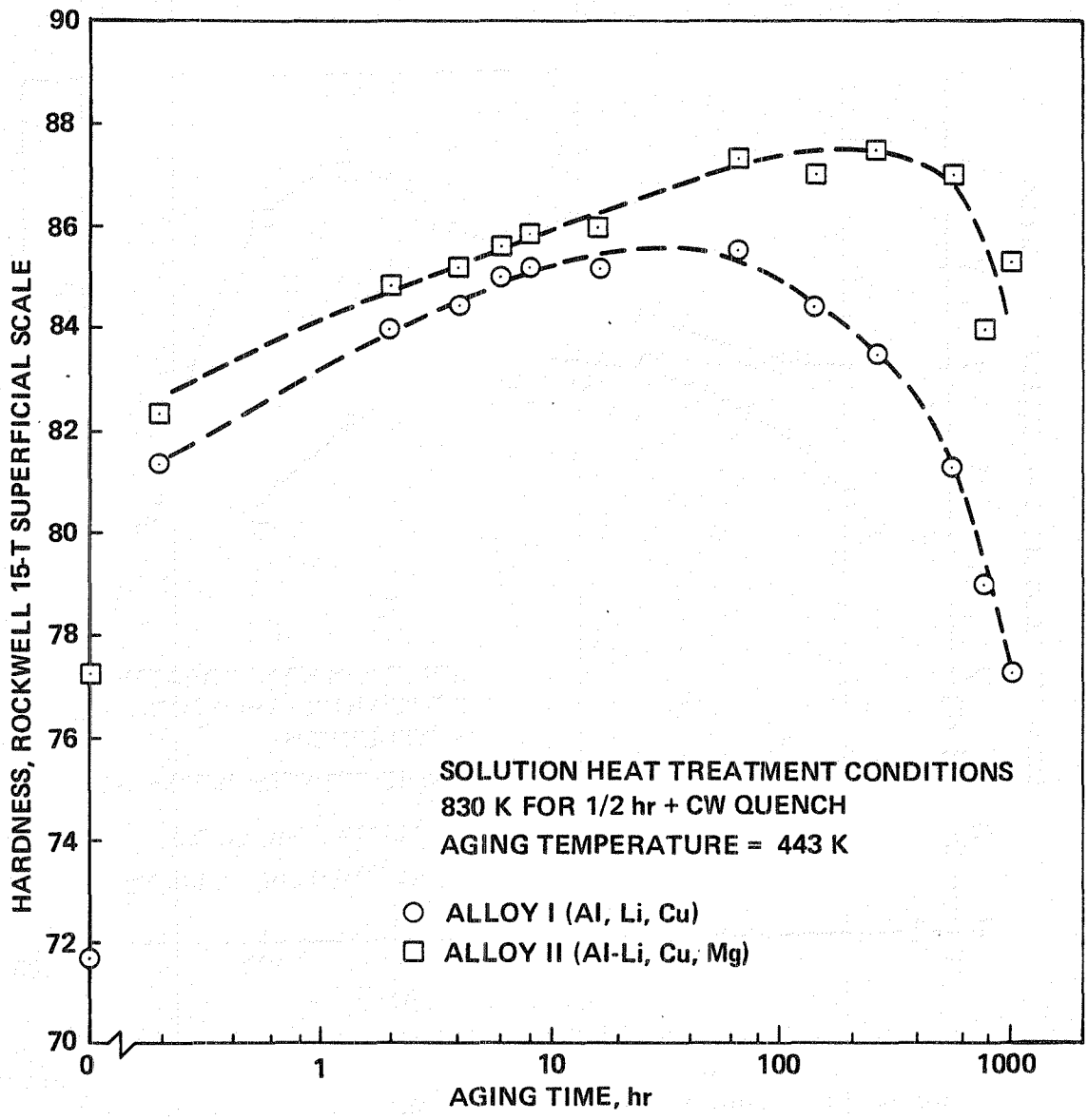

Fig. 8: Aging response of Alloys I and II at 443K (170C): hardness as a function of the time of aging.

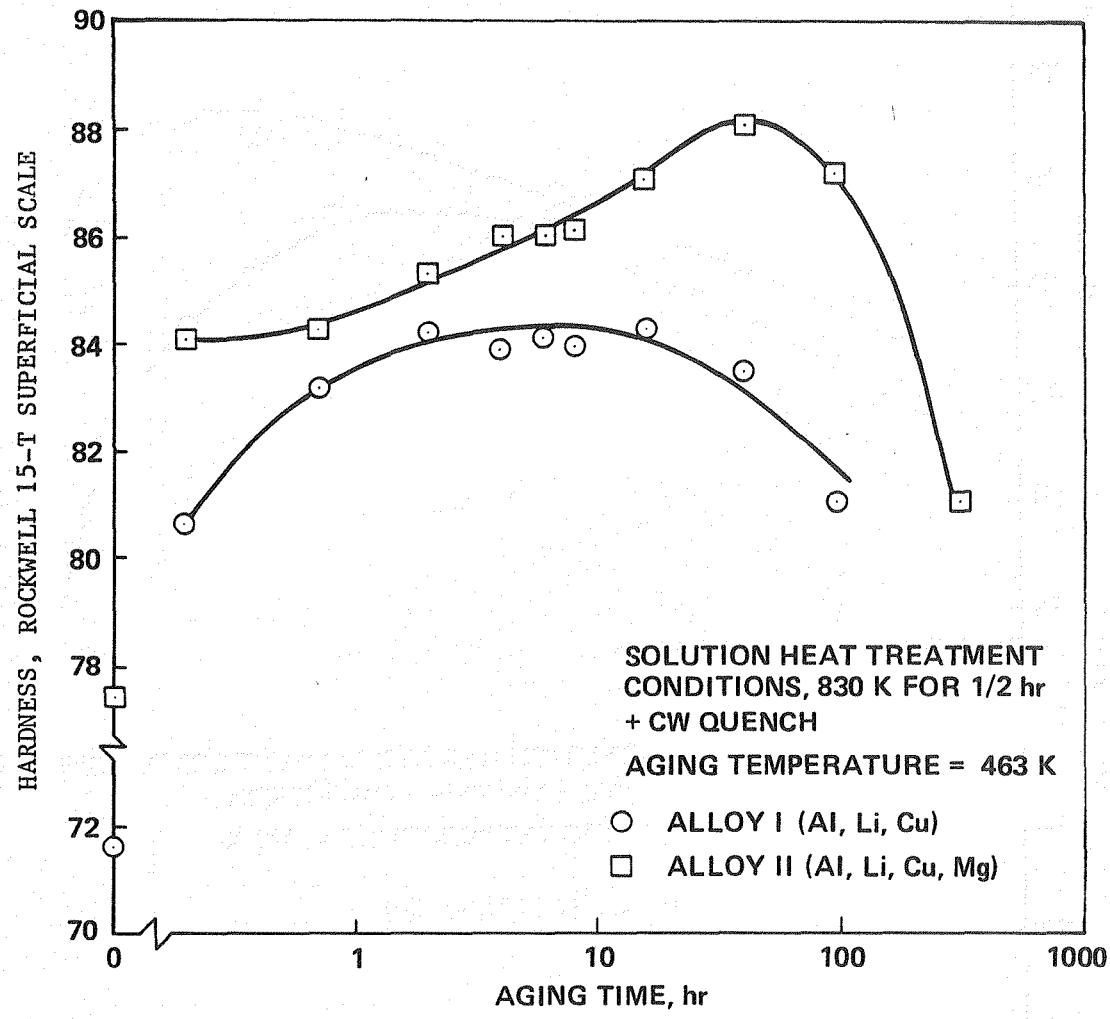

Fig. 9: Aging response of Alloys I and II at 463K (190C): hardness as a function of the time of aging.

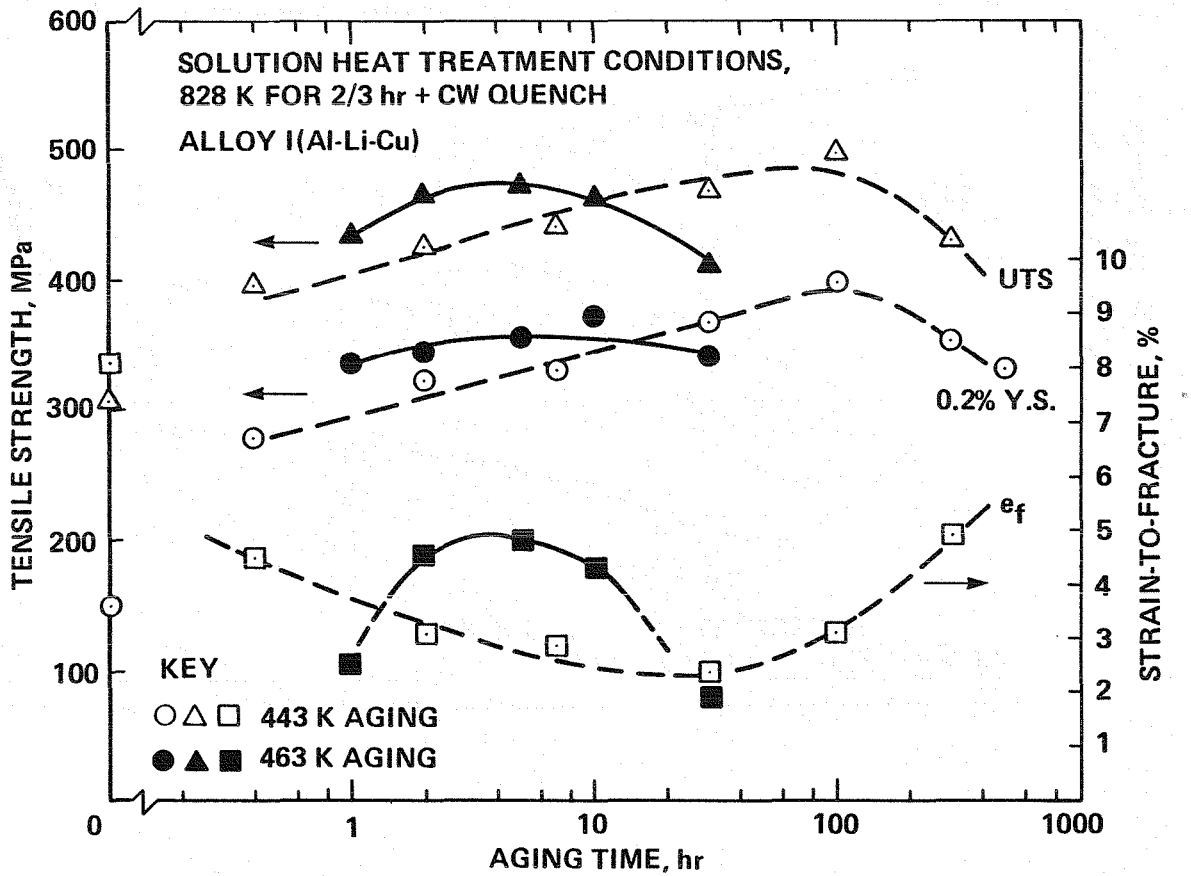

Fig. 10: Aging response of Alloy I hot-rolled sheet: tensile properties as a function of aging time at two aging temperatures - 443K and 463K.

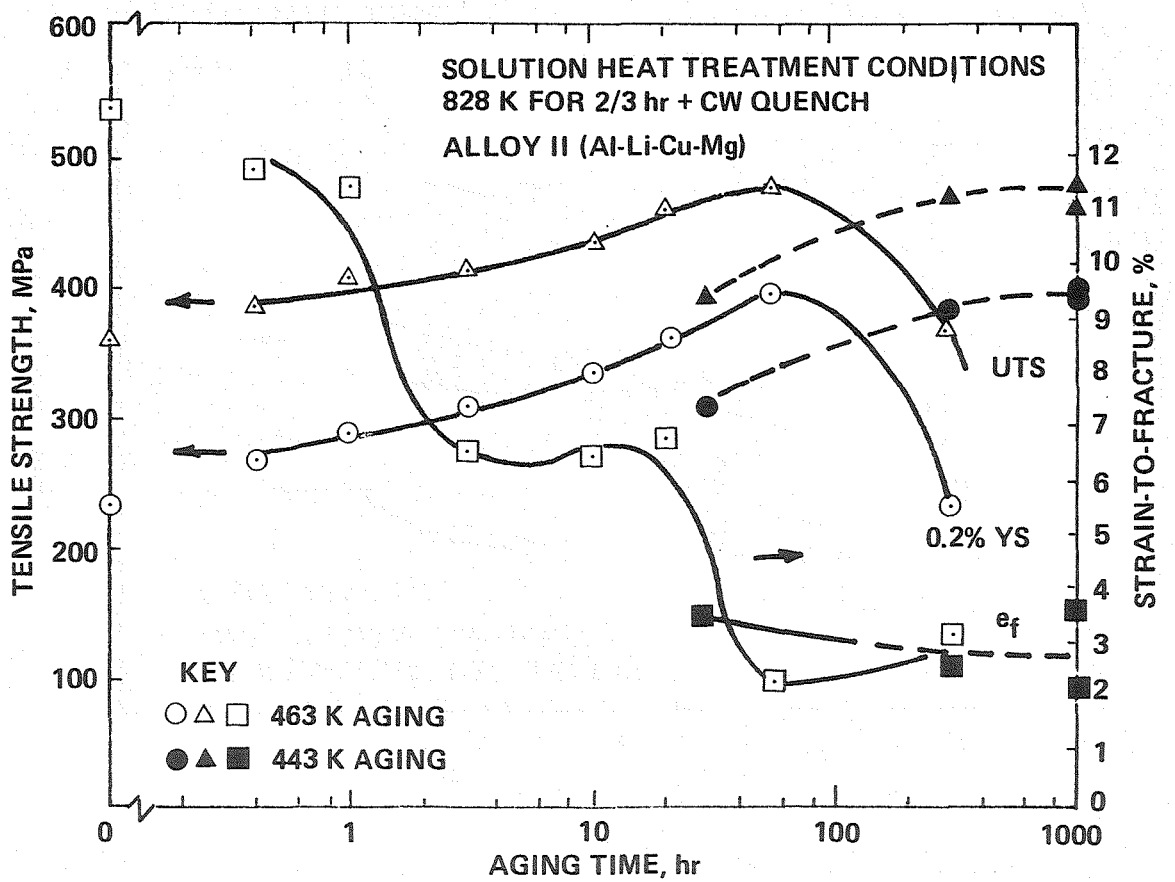

Fig. 11: Aging response of Alloy II hot-rolled sheet: tensile properties as a function of aging time at two aging temperatures - 443K and 463K.

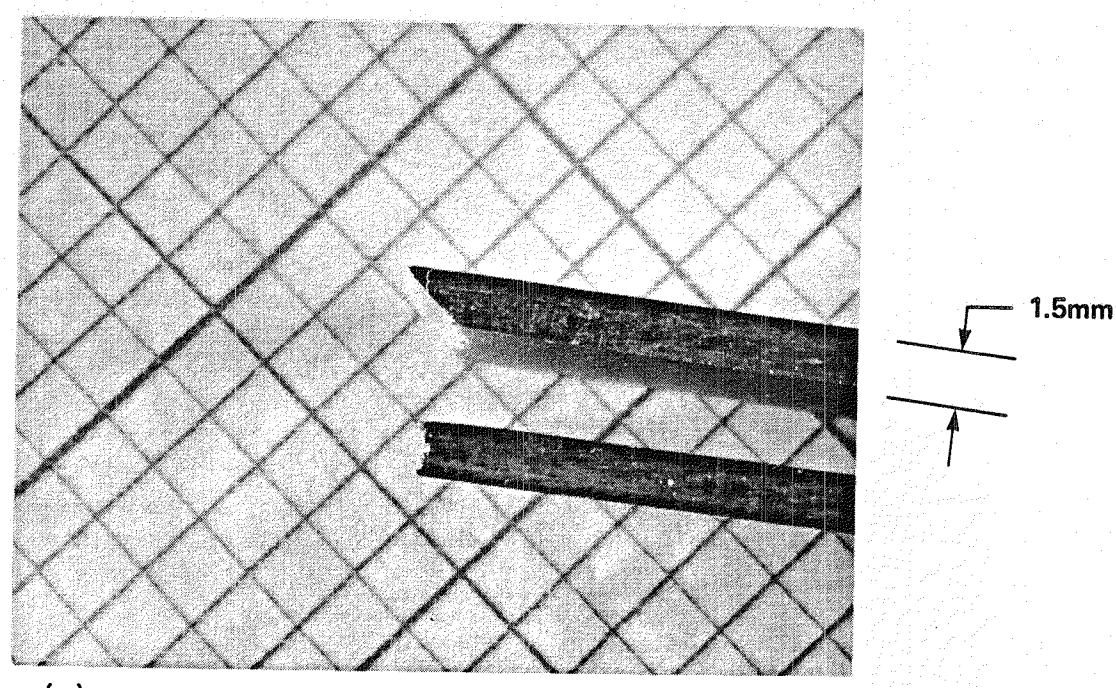

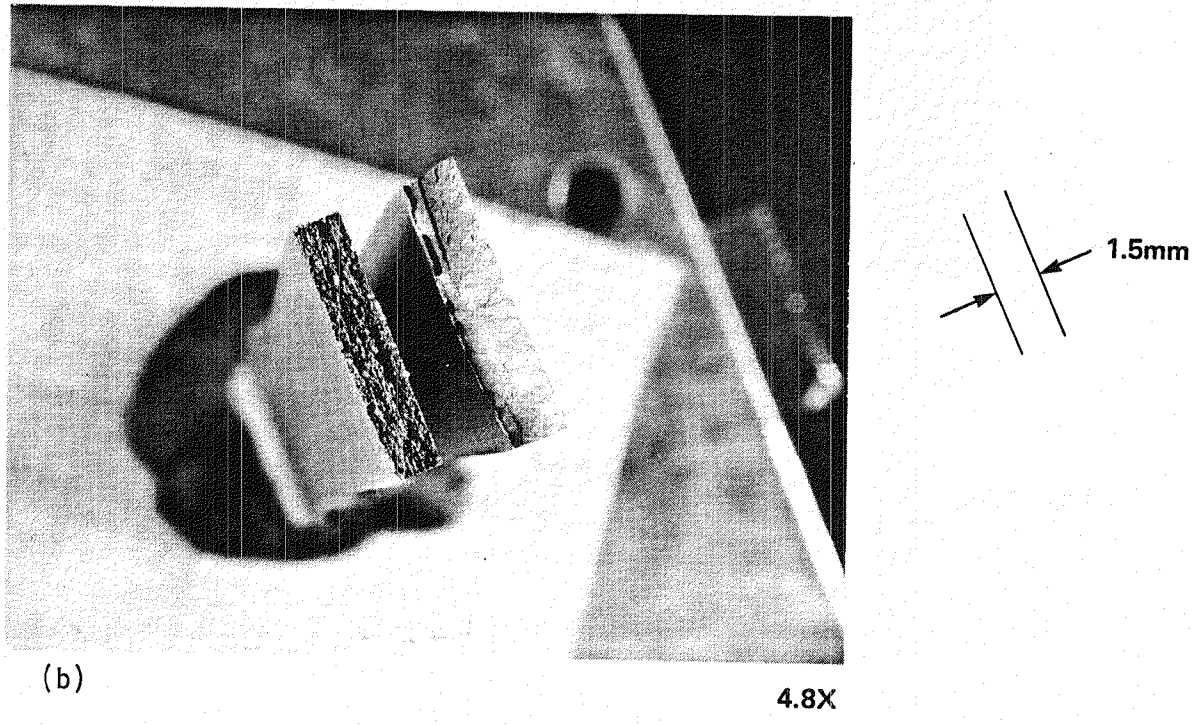

Fig. 12: The fracture morphology of tensile coupons fabricated from the hot-rolled strip (a) fracture profile, Alloy I (upper) versus Alloy II (lower) and (b) fracture surface comparison, Alloy I (right) versus Alloy II (left).

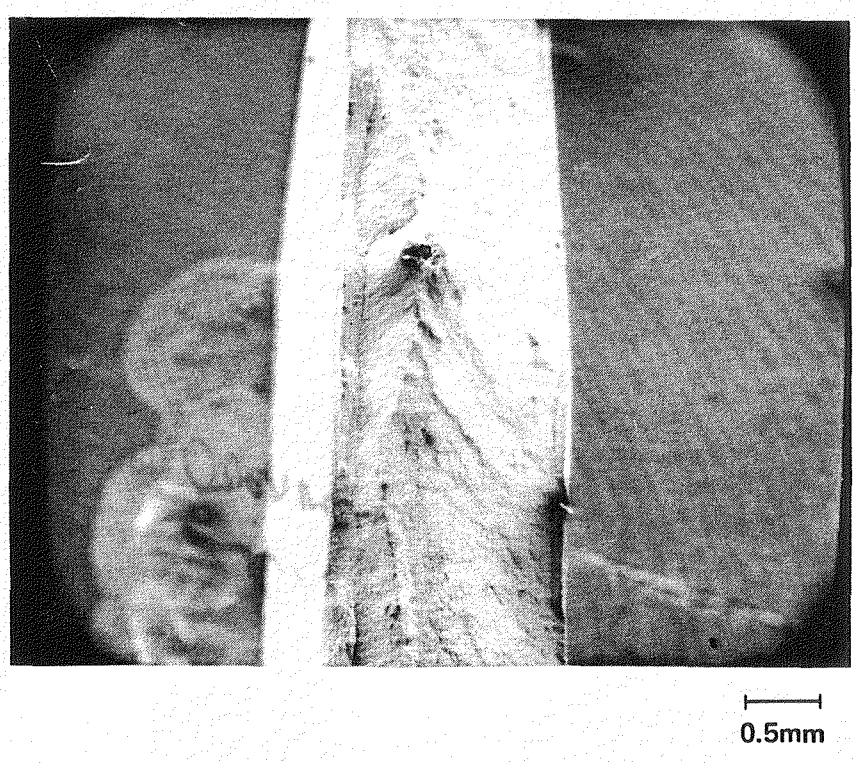

Fig. 13: Scanning electron micrograph (SEM) of a fracture representative of that found for the hot-rolled Alloy I tensile coupons.

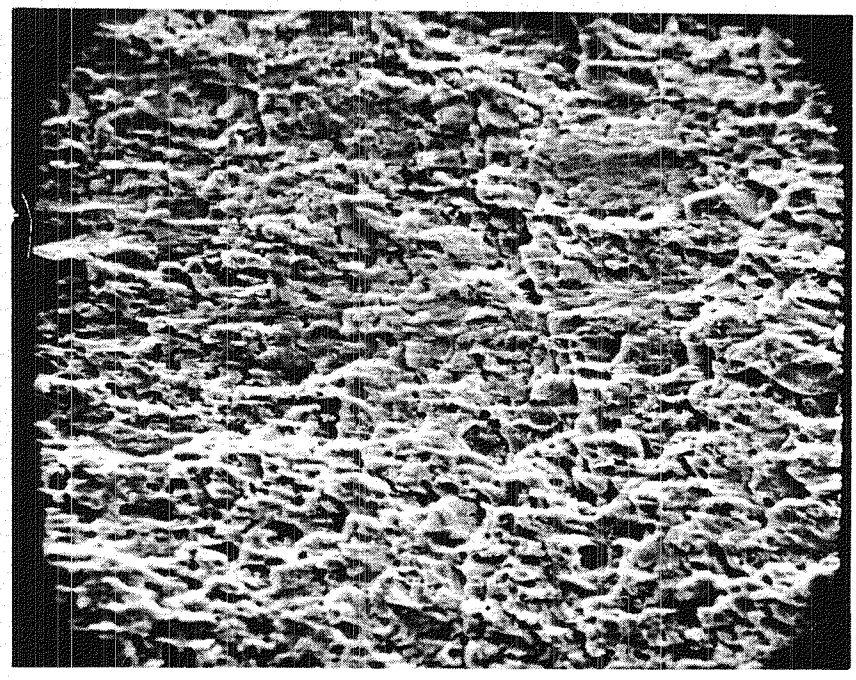

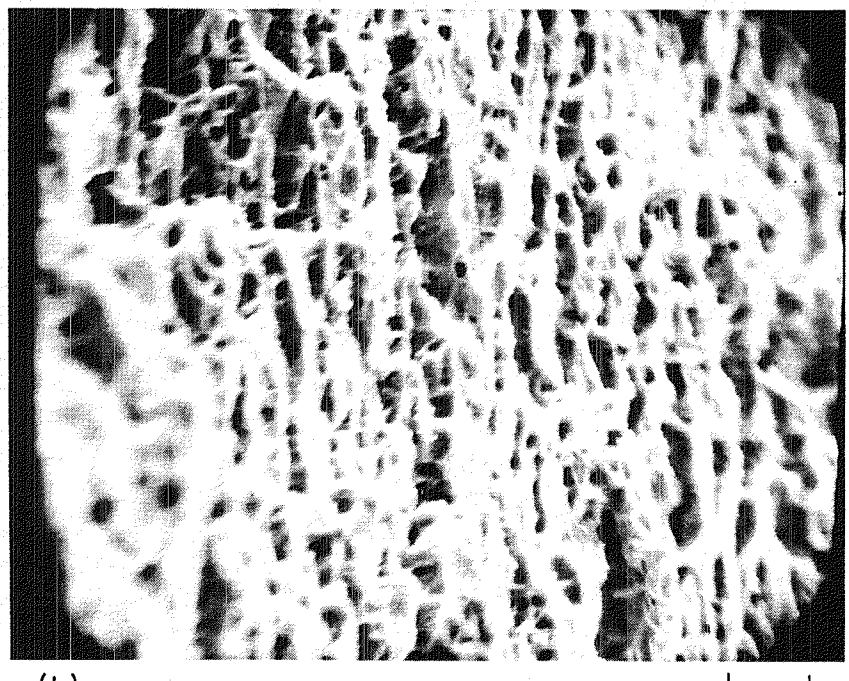

Fig. 14: Representative fractography (SEM) of the hot-rolled Alloy I tensile fractures (a) characteristic fracture topography (b) stepped features as viewed with side-tilt.

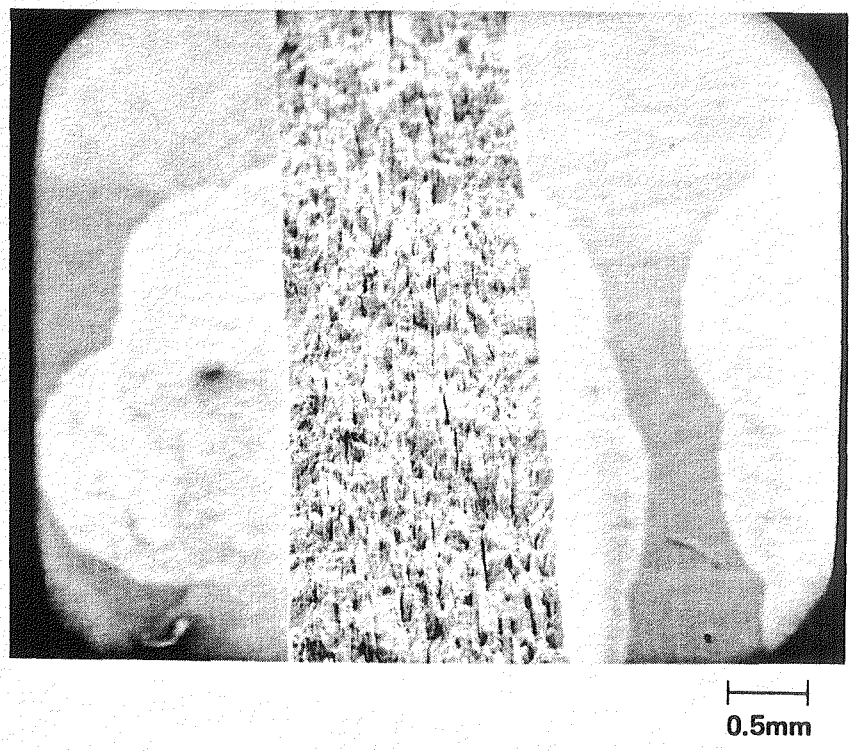

Fig. 15: Scanning electron micrograph (SEM) of a fracture representative of that obtained in the hot-rolled Alloy II (magnesium bearing) tensile coupons.

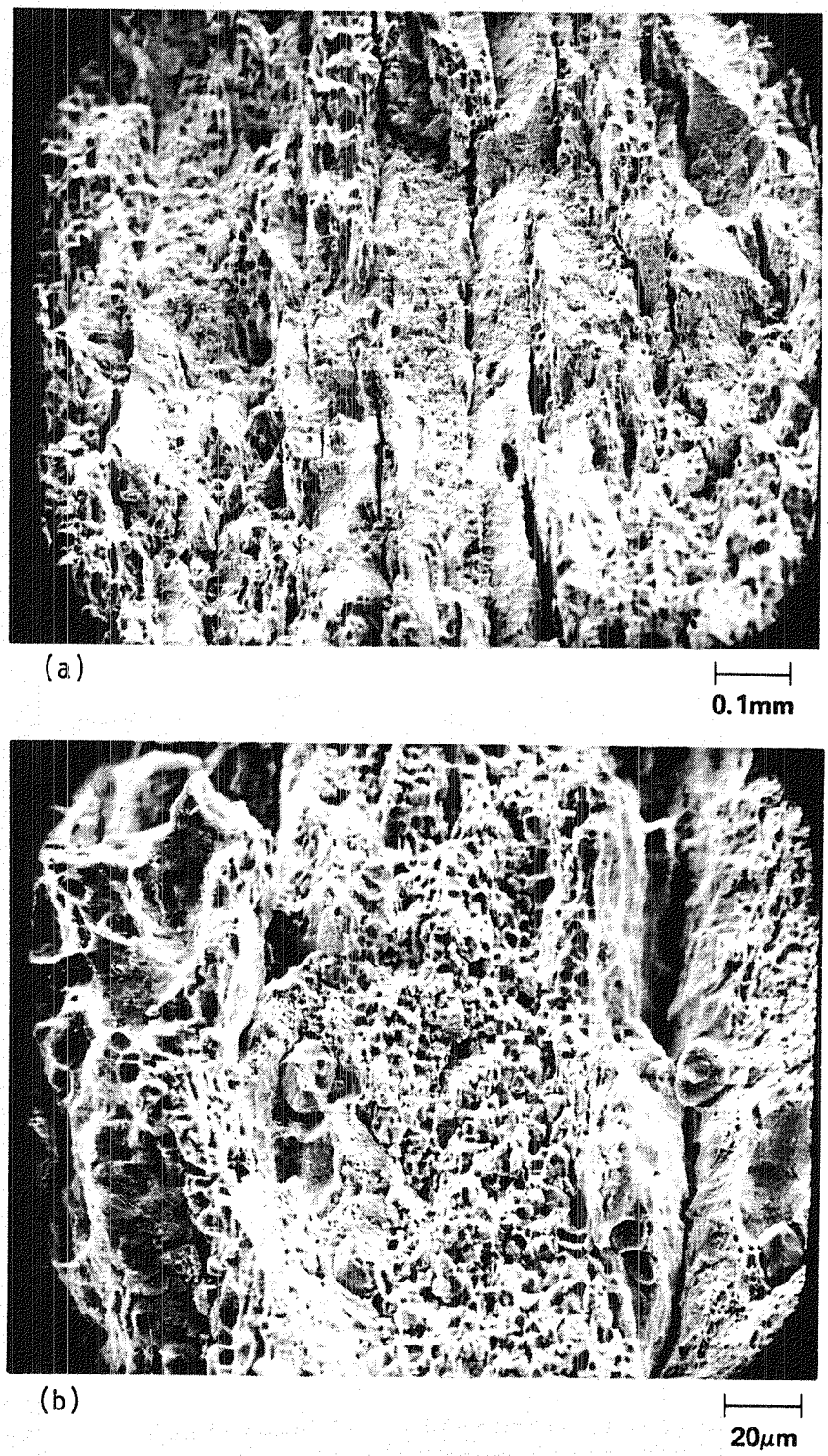

Fig. 16: Representative fractography (SEM) of the hot-rolled Alloy II tensile fractures (a) high magnification of the fracture depicted in Fig. 15 (b) further magnification of the fracture (center region depicted in micrograph (a).

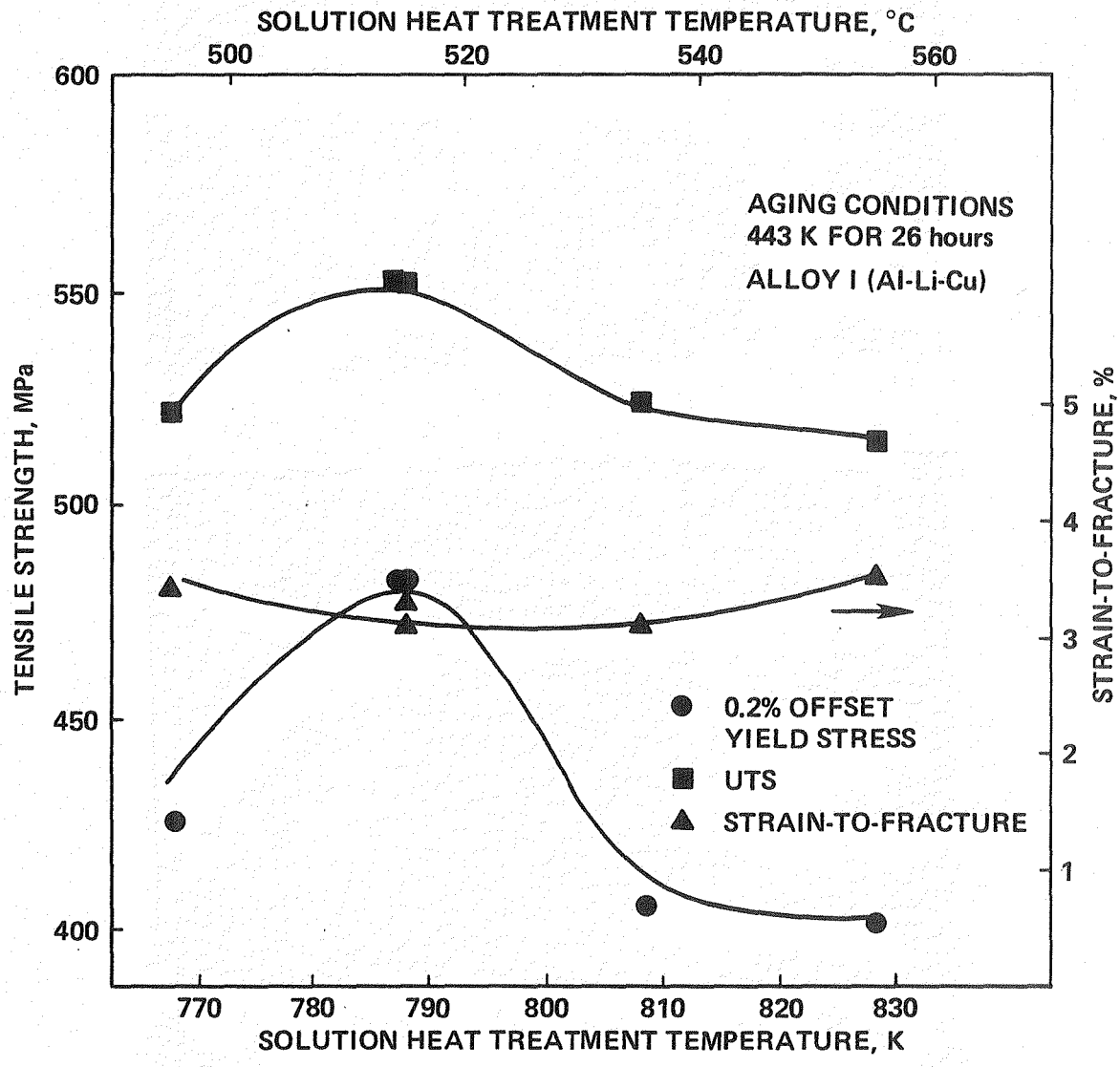

Fig. 17: The effect of solution heat treatment temperature on the tensile properties of as-extruded Alloy I for a constant aging condition.

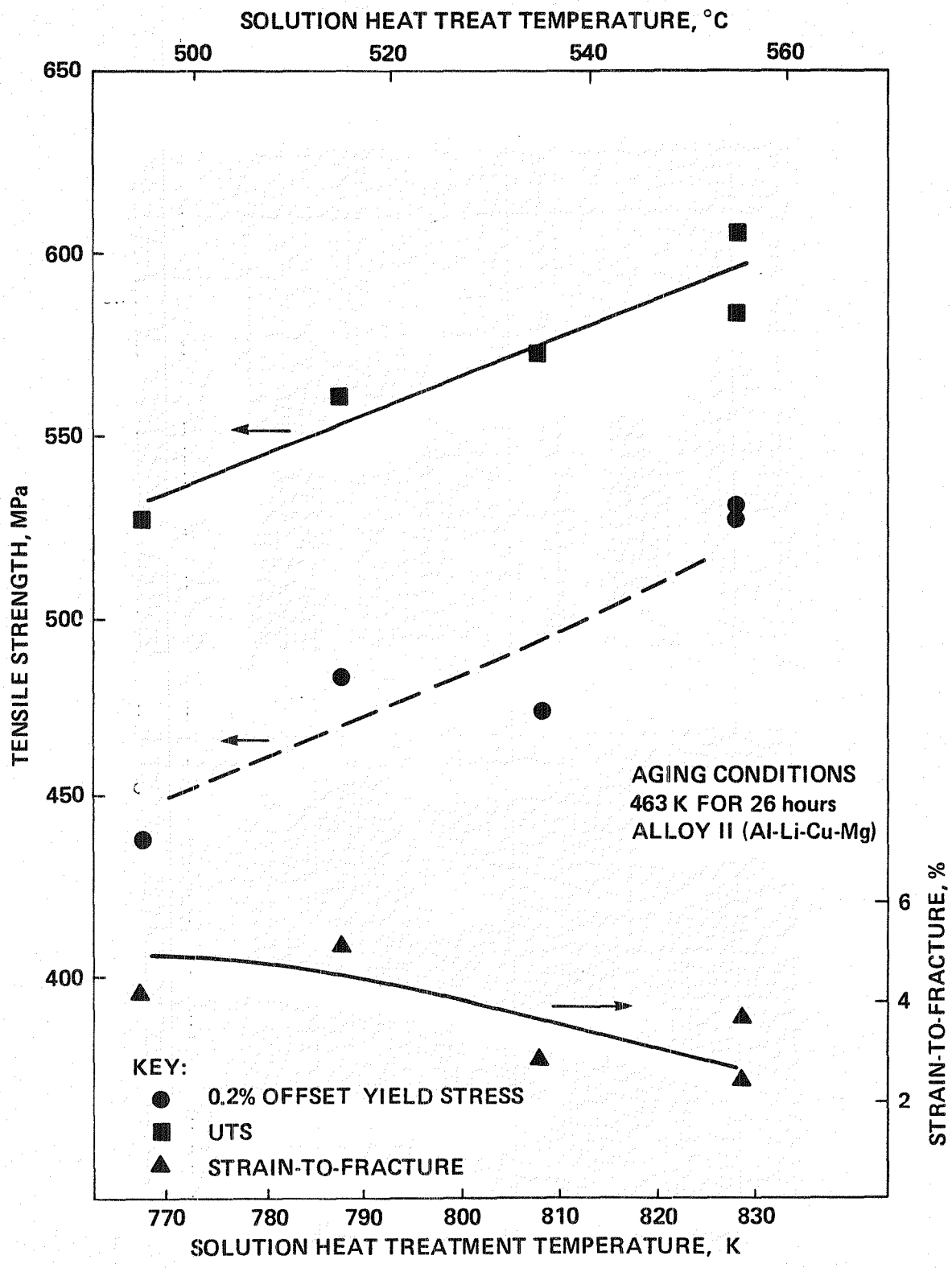

Fig. 18: The effect of solution heat treatment temperature on the tensile properties of as-extruded Alloy II for a constant aging condition.

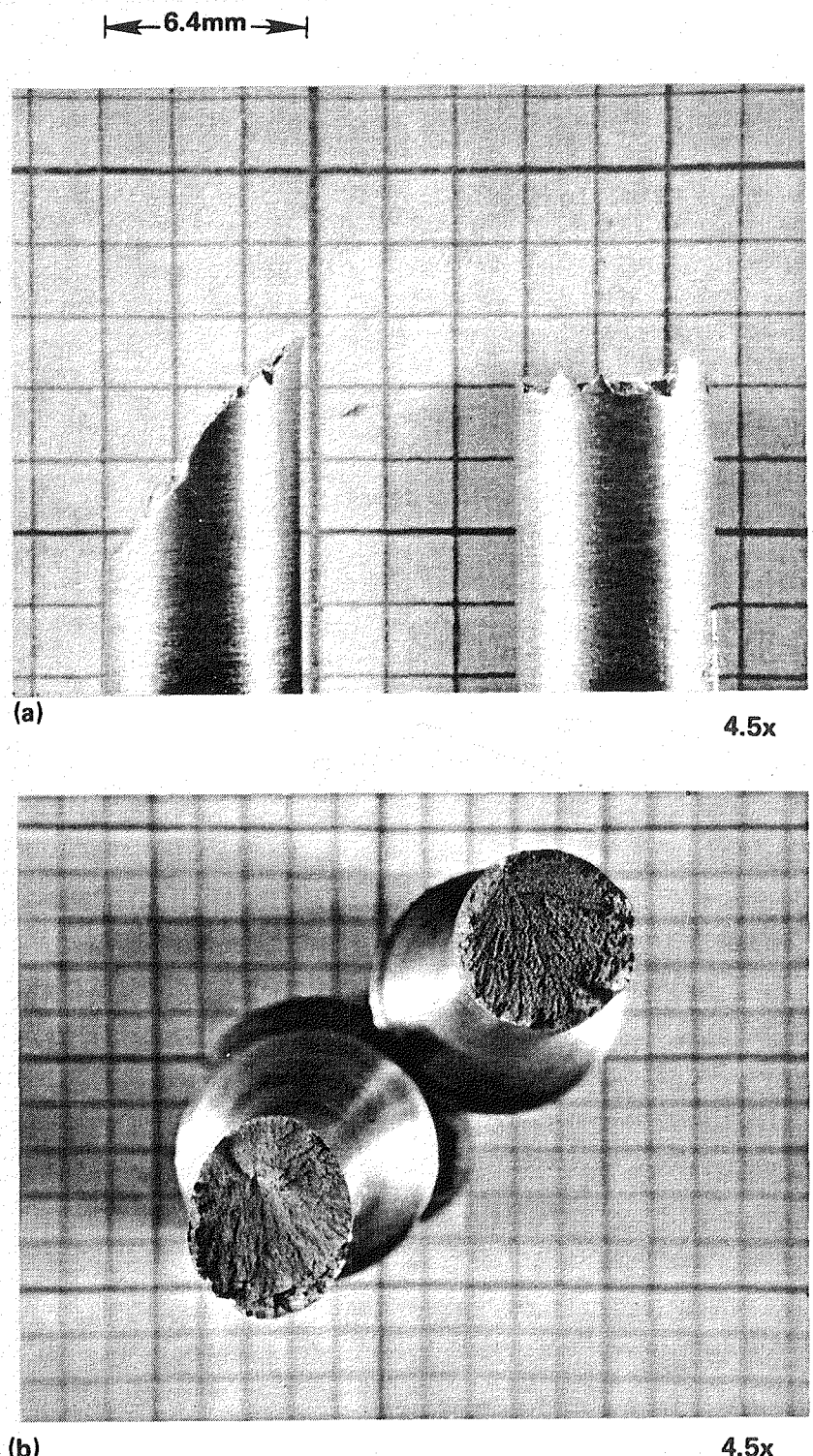

Fig. 19: The fracture morphology of tensile rounds fabricated from the as-extruded plate (a) fracture profile Alloy I (left) versus Alloy II (right) and (b) fracture surface comparison, Alloy I (left) versus Alloy II (right).

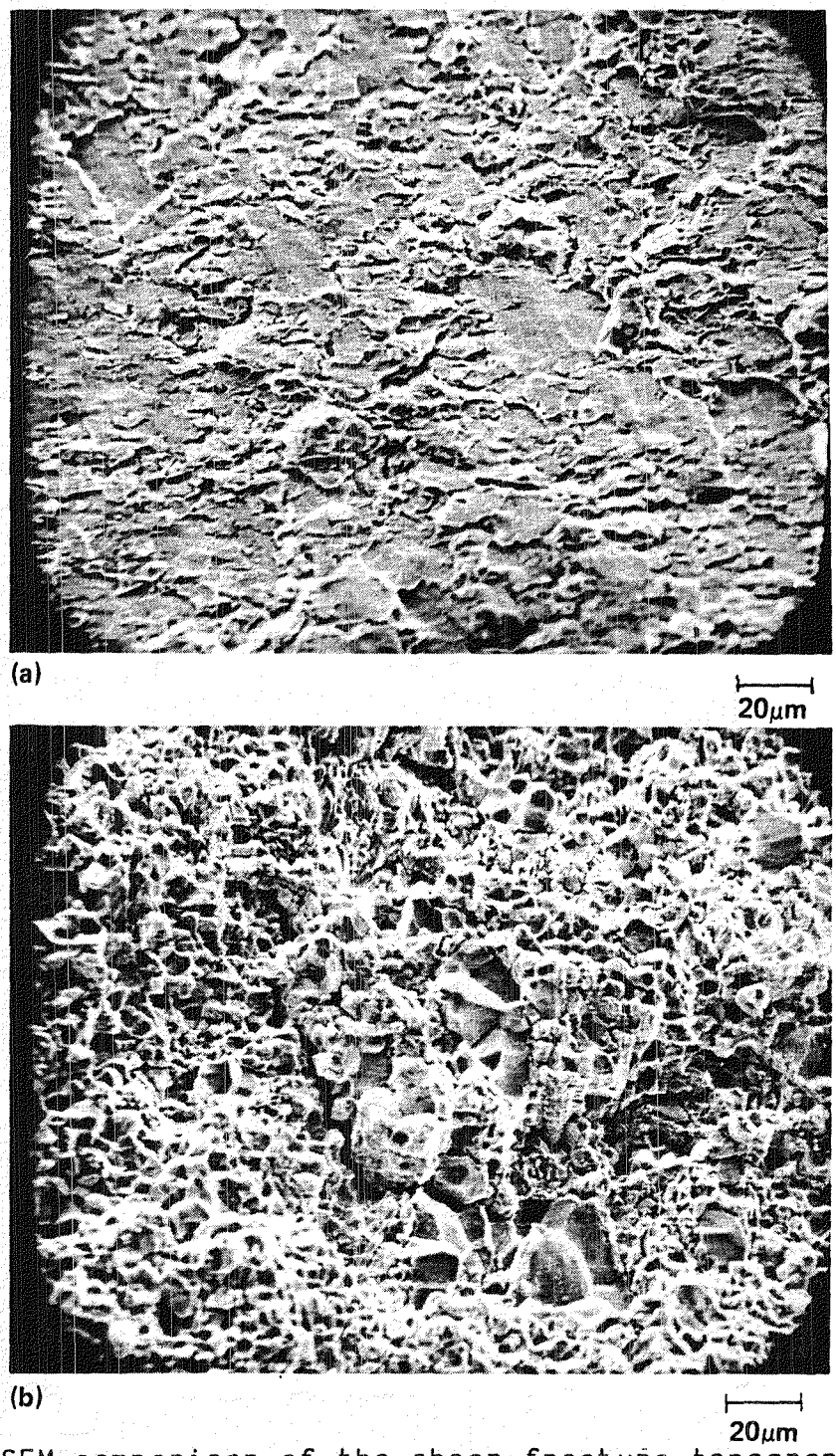

Fig. 20: SEM comparison of the shear fracture topography, Alloy I, to the tensile fracture topography of Alloy II for tensile round specimens fabricated from the as-extruded plate (a) stepped shear topography characteristic of Alloy I (b) intergranular fracture observed in Alloy II.

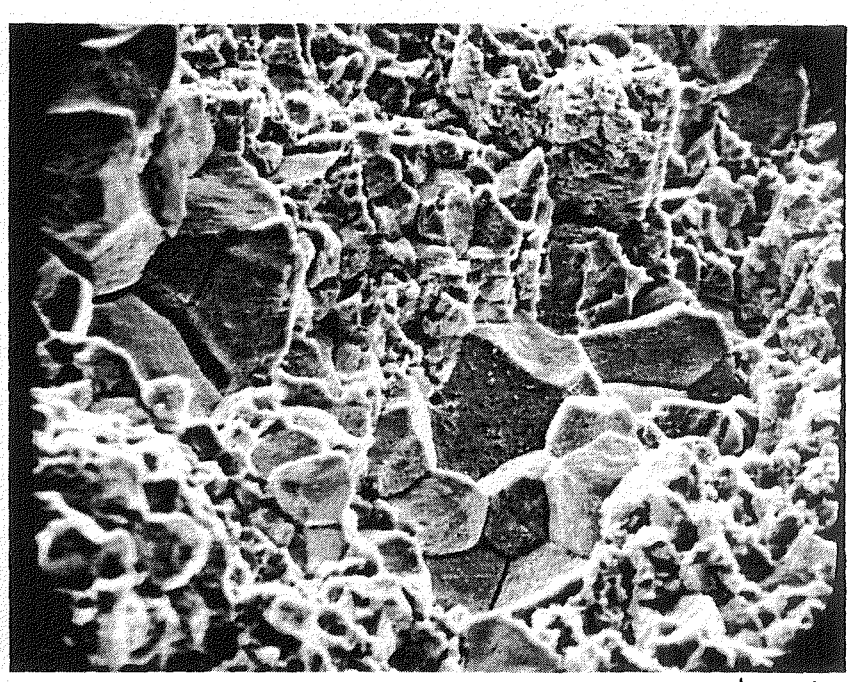

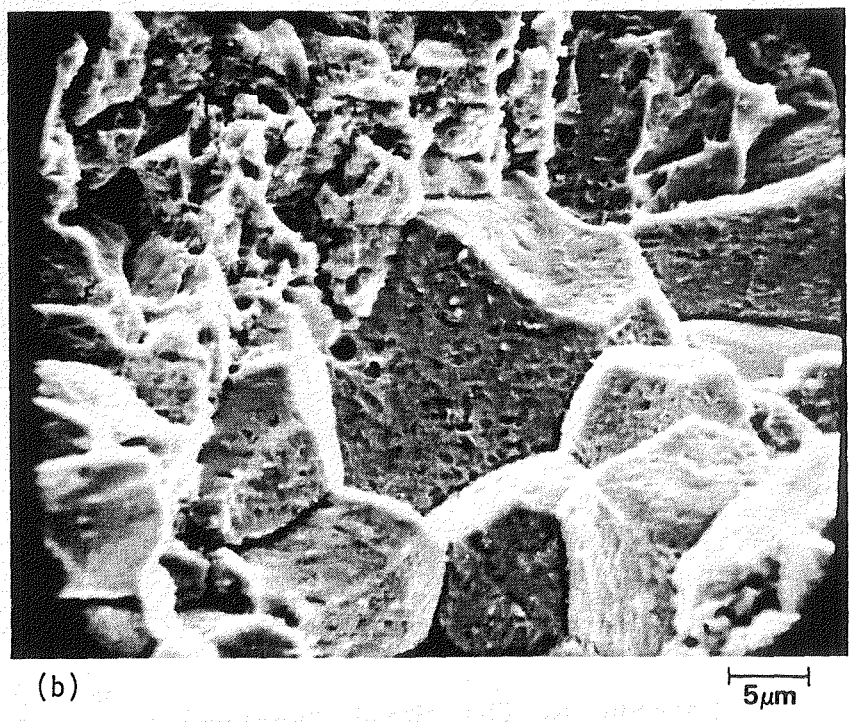

Fig. 21: Intergranular fracture of Alloy II (Al-Li-Cu-Mg) (a) intergranular facets and secondary cracks (b) two-fold magnification of the faceted region in (a), above, depicting extensive grain boundary precipitation.

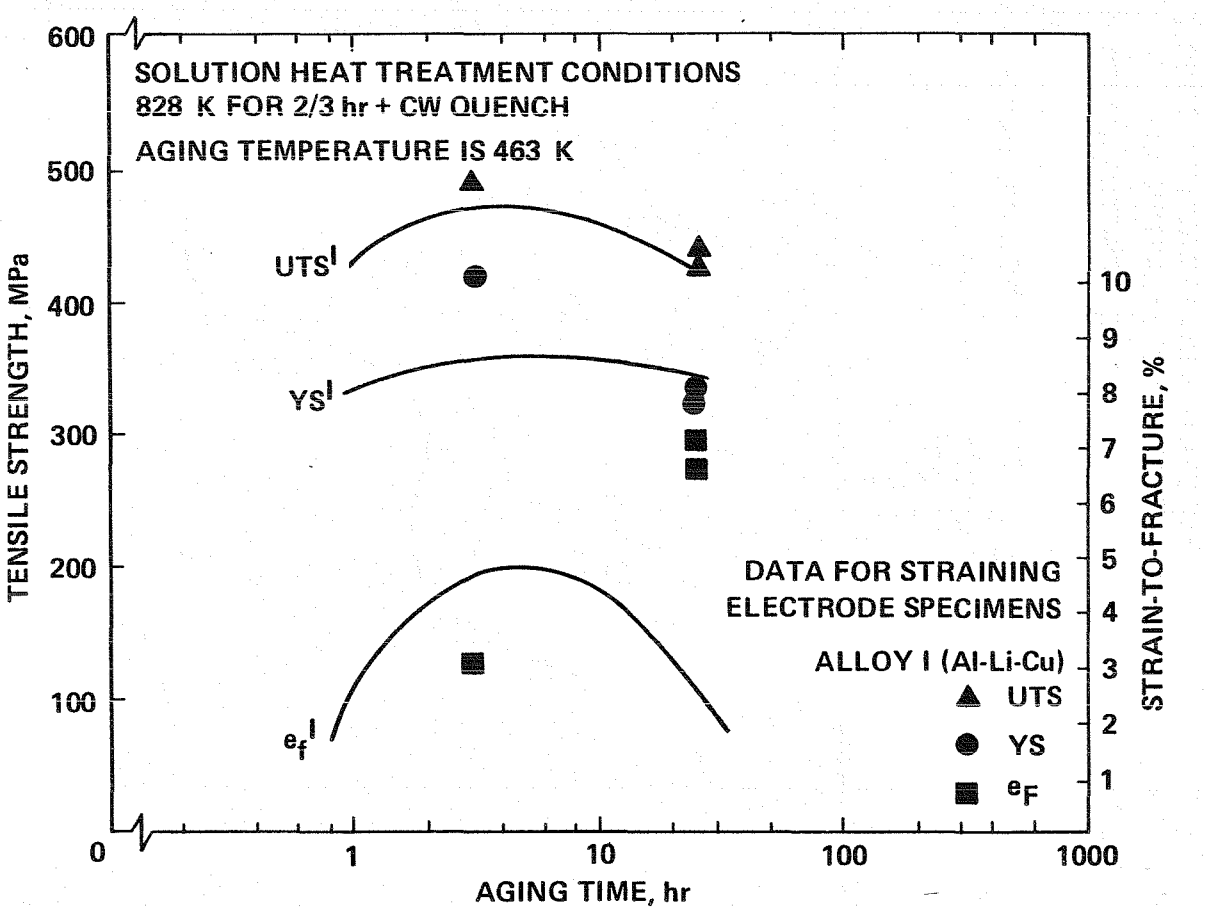

Fig. 22: A comparison of Alloy I straining electrode specimen data to the aging response curves obtained from tensile coupons, Fig. 10.

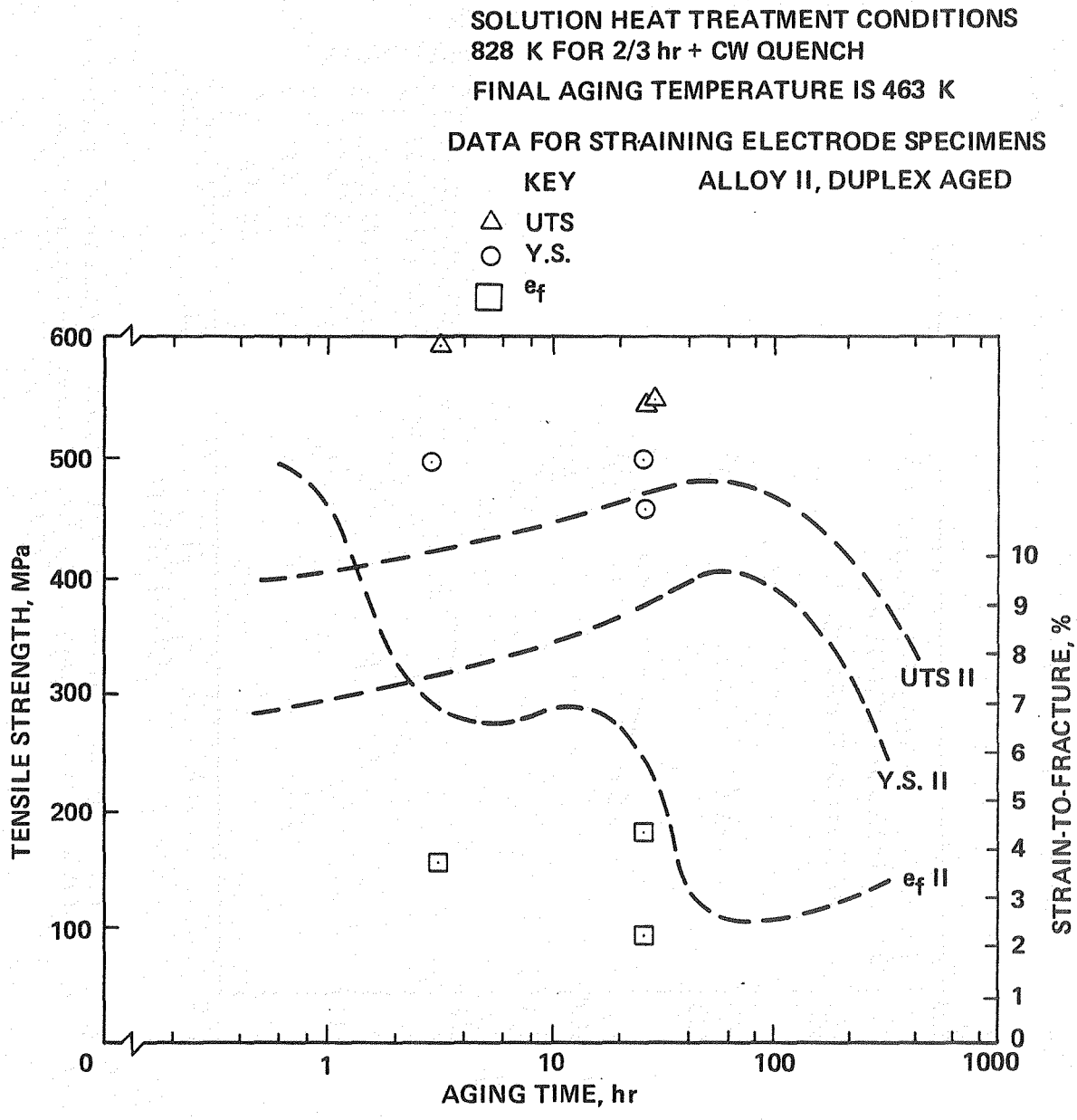

Fig. 23: A comparison of Alloy II straining electrode specimen data to the aging response curves obtained from tensile coupons, Fig. 11.

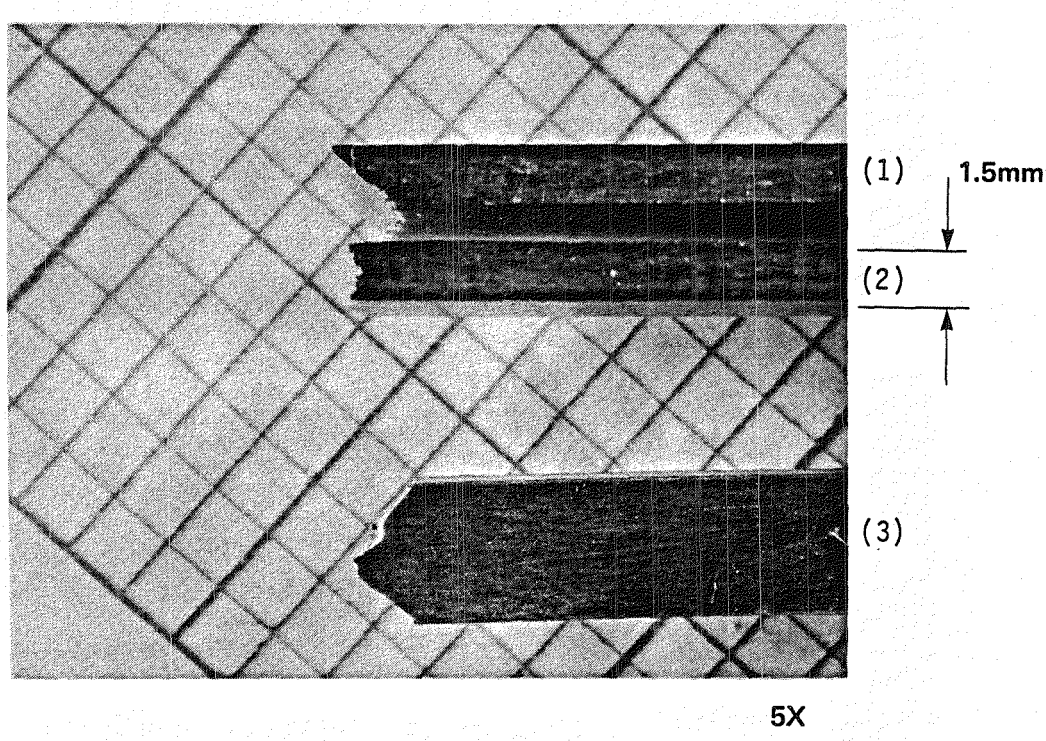

Fig. 24: A comparison of fracture profiles of three specimens (1) shear fracture of an Alloy I tensile coupon (top) (2) tensile fracture and an Alloy II tensile coupon (center), and (3) double shear fracture of a straining electrode type specimen, Alloy I (bottom).

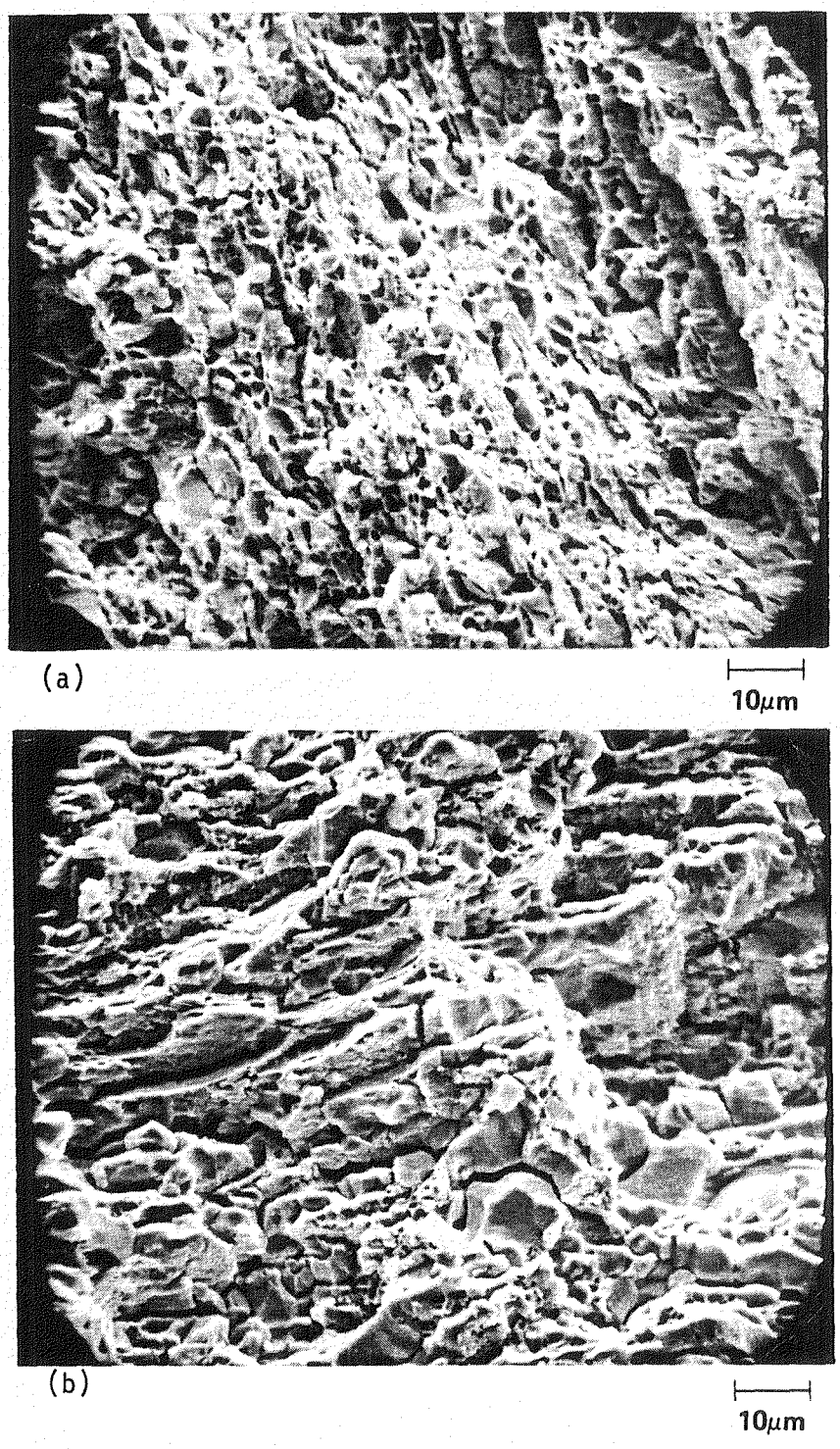

Fig. 25: SEM comparison of the shear fracture topography, Alloy I, to the tensile fracture topography of Alloy II for straining electrode specimens fabricated from the as-extruded plate (a) stepped shear topography, Alloy I (b) grain boundary faceting and secondary cracking, characteristic of Alloy II.

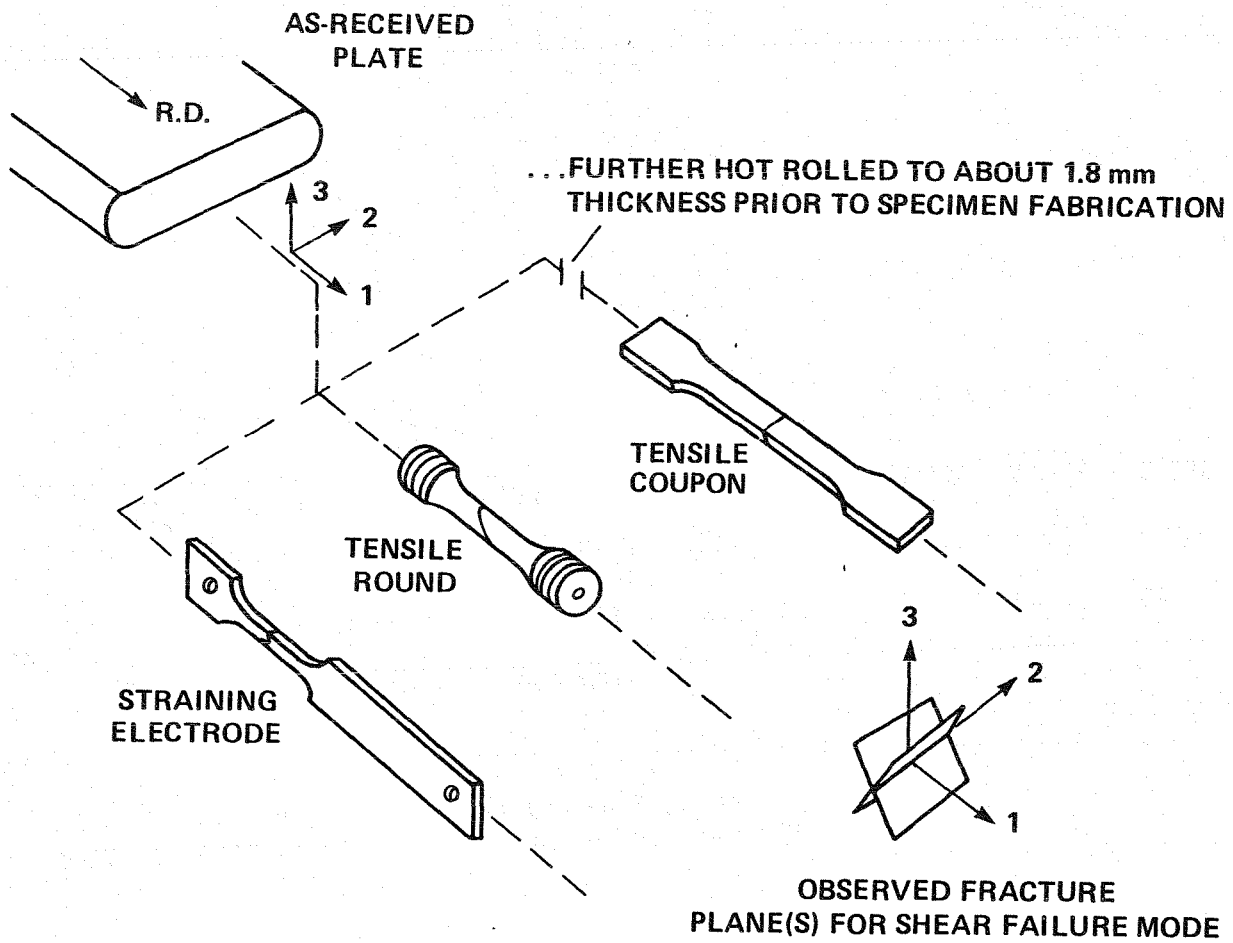

Fig. 26: The orientational relationship between the shear fracture plane(s) and the extrusion direction (E.D.) of the as-received Al-Li alloy plate.

Table I Chemical Composition of the Aluminum-Lithium Alloys Selected for this Study

Program Designation	KBI Alloy Designation	Wt. Pct.											ppm		
		Li	Cu	Mg	Zr	Si	Fe	Mn	Zn	Ti	Cr	Be	Ca	Na	K
Alloy I	80001	2.6	1.4	.006	.09	.03	.06	<.005	<.02	<.03	<.002	<.005	<3	2	1
Alloy II	80002	2.6	1.4	1.6	.09	.03	.05	<.005	<.02	<.03	<.002	<.005	<3	1	1

Table II Young's Modulus Comparison Data

$E_{\text{Alloy I}}$	=	80.0 GPa
$E_{\text{Alloy II}}$	=	80.7 GPa
$E_{\text{7075-T6 Aluminium}}$	=	71.7 GPa

Note: a) Alloys I and II in peak-aged condition.

b) Modulus determinations made from the output of two strain gages on opposite sides of flat tensile coupons.

c) 7075-T6 Modulus value reported in Aluminum Standards and Data - 1979, The Aluminum Association (Sixth Edition), March 1979.

1. Report No.	2. Government Accession No.	3. Recipient's Catalog No.
NASA CR-166339		

4. Title and Subtitle	5. Report Date
THE RELATIVE STRESS-CORROSION-CRACKING SUSCEPTIBILITY OF CANDIDATE ALUMINUM-LITHIUM ALLOYS FOR AEROSPACE STRUCTURAL APPLICATIONS	September 1980
	6. Performing Organization Code
7. Author(s) Patrick P. Pizzo	8. Performing Organization Report No. TR-45-1
	10. Work Unit No.
9. Performing Organization Name and Address Advanced Research and Applications Corporation 1223 E. Arques Avenue Sunnyvale, California 94086	11. Contract or Grant No. NAS2-10365
	13. Type of Report and Period Covered Contractor report
12. Sponsoring Agency Name and Address National Aeronautics and Space Administration Washington, DC 20546	14. Sponsoring Agency Code

15. Supplementary Notes

Ames Technical Monitor: Howard G. Nelson, NASA Ames Research Center Moffett Field, Ca 94035, (415) 965-6137/FTS448-6137

Annual Report

16. Abstract

The microstructure and tensile properties of two powder metallurgy processed aluminum-lithium alloys have been determined. The alloy composition are Alloy I: Al-2.6% Li-1.4% Cu and Alloy II: Al-2.6% Li-1.4% Cu-1.6% Mg. Strength properties of 480 MPa yield and 550 MPa ultimate tensile strength with 5% strain-to-fracture were attained. However, very little reduction-in-area was observed and fracture characteristics were brittle. The magnesium bearing alloy exhibited the highest strength and ductility, but fracture was intergranular. Recrystallization and grain growth, as well as coarse grain boundary precipitation, occurred in Alloy II. The fracture morphology of the two alloys differed. Alloy I fractured along a plane of maximum shear stress, while Alloy II fractured along a plane of maximum tensile stress. A fixed orientational relationship exists between the shear fracture plane and the rolling direction; thus, suggesting that the PM alloys are strongly textured.

17. Key Words (Suggested by Author(s))	18. Distribution Statement
P/M alloys, advanced Al-Li alloys, mechanical characterization, fracture morphology, microstructure.	Unlimited - Unclassified STAR Category - 26

19. Security Classif. (of this report)	20. Security Classif. (of this page)	21. No. of Pages	22. Price*
Unclassified	Unclassified	58	

*For sale by the National Technical Information Service, Springfield, Virginia 22161

End of Document